

## CHAPTER - 3

### CORROSION INHIBITION CHARACTERISTICS OF ISOXAZOLINE DERIVATIVES FOR MILD STEEL IN 1M H<sub>2</sub>SO<sub>4</sub>

---

---

#### 3.1 INTRODUCTION

Corrosion is one of the most serious problems in the world, especially in an industry causing several material and financial losses. Mild steel (MS) is a promising material used for various industrial applications such as reactors, petrochemical process devices, boilers, drums and heat exchangers. However, exposure of MS with aqueous acidic solution during descaling, acid pickling and acid treatment in oil industries causes corrosion. In efforts to diminish electrochemical corrosion, the primary strategy is to isolate the metal from corrosive media. Several methods are available, but the use of chemical corrosion inhibitors is one of the most appropriate and economical way to achieve this target<sup>1</sup>.

In order to tackle the menace attributed to corrosion, several measures (including anodic and cathodic protection, lubrication, painting and electroplating) have been adopted. However, one of the best options accessible for the protection of metals against corrosion involves the use of organic inhibitor<sup>2</sup>. Most successful inhibitors are synthesized from cheap raw materials or selected from compounds, which have hetero atom (N, O, P and S) in their aromatic or long carbon chain<sup>3</sup>. The inhibition efficiency follows the sequence O < N < S < P. The interactions between an organic inhibitor and a metal surface are principally physical adsorption and/or chemisorption. Sulphur and/or nitrogen containing heterocyclic compounds are considered to be effective corrosion inhibitors. Beside amine compounds widely studied in corrosion protection, thiophene derivatives also offer special affinity to inhibit corrosion of metals in acid solutions. S and/or N atoms adsorb easily on metal surface displacing water molecules as suggested by **Bouklah**<sup>4</sup>. Nitrogen-containing heterocyclic compounds are considered to be effective corrosion inhibitors<sup>5</sup> and function *via.*, adsorption of the molecules on the metal surface creating a barrier to corrosive attack. The phenomenon of adsorption is influenced by the nature and surface charge of metal, type of aggressive medium and chemical structure of inhibitors. The adsorption process depends mainly on physicochemical properties of the

molecule such as functional groups, steric factor, molecular size, molecular weight, molecular structure, aromaticity, electron density of the donor atoms and orbital character of donating  $\pi$  electrons<sup>6</sup>.

Isoxazolines are five membered heterocyclic organic compounds that contain oxygen and nitrogen atoms. Substituted isoxazoline derivatives are an important class of heterocyclic compounds which possess a wide range of applications such as pharmaceutical, agrochemical agents and medicinal research. A large number of isoxazolines containing penicillin derivatives are found to be antibacterial. These are also used as corrosion inhibitors for fuels and lubricants and show good potency in animal lubricants<sup>7</sup>. A thorough review of literature revealed that not much work has been reported on the use of isoxazoline derivatives as corrosion inhibitors. This motivated us to take up this research problem, where some isoxazolines have been synthesized and evaluated for their corrosion inhibition property.

The efficiency of the isoxazoline derivatives have been evaluated by electrochemical and non-electrochemical techniques. The efficiency of these derivatives have been verified by some spectroscopic methods such as FTIR spectroscopy, SEM-EDS, XRD and AFM. Recently, quantum chemical calculations have been performed enormously to complement the experimental evidences<sup>8</sup>. Density functional theory has been applied widely to compute electronic properties possibly relevant to the inhibition action. Knowing the orientation of the molecule, favourable configurations, atomic charges, steric and electronic effects would be useful for better understanding of the inhibitor performance. The experimental data can be correlated well with quantum chemical parameters such as hardness, softness, highest occupied (HOMO) and lowest unoccupied (LUMO) molecular orbital energies and the energy gap between them<sup>9</sup>. Keeping the above facts in view, non-electrochemical, electrochemical, spectroscopic and DFT methods have been selected to evaluate the inhibition efficiency of the synthesized isoxazolines.

## 3.2 EXPERIMENTAL WORK

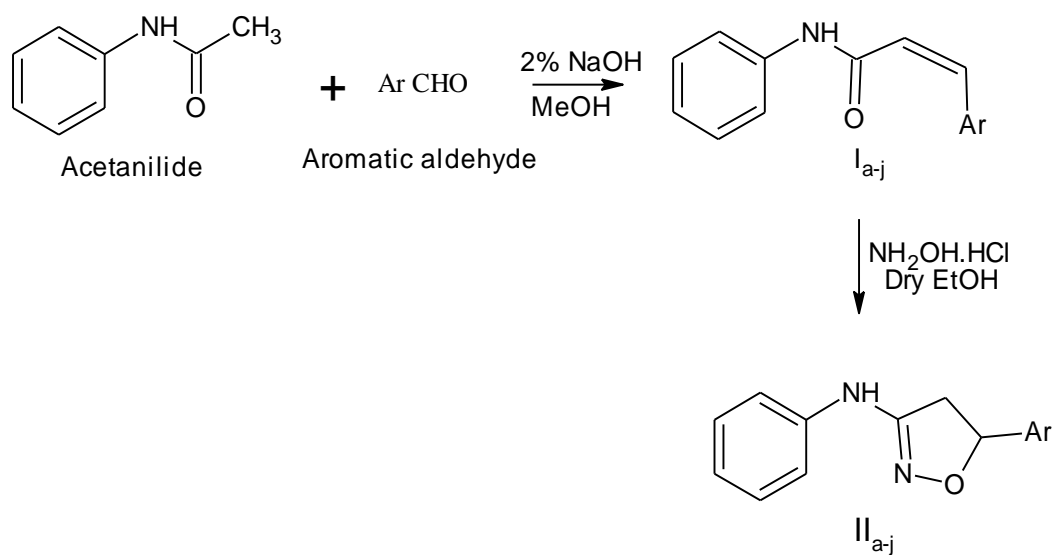
### 3.2.1 Synthesis of inhibitors

#### (i) Synthesis of chalcones (I<sub>a-j</sub>)

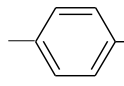
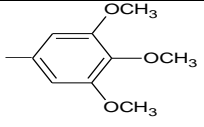
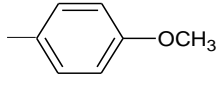
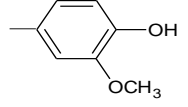
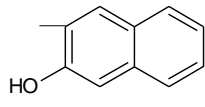
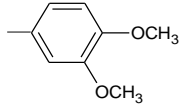
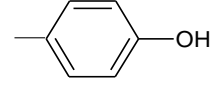
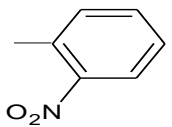
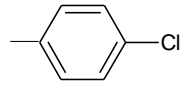
Chalcones were prepared by reacting a mixture of acetanilide (0.05 mol), aromatic aldehyde (0.05 mol), aq. sodium hydroxide (10 %, 5 ml) and methanol (50 ml). The reaction mixture was stirred for 10 hours at room temperature using magnetic stirrer. Then, it was refluxed for further 6 hours on a water bath. After completion of the reaction, excess solvent was removed by distillation and the resultant viscous mass was poured into ice water with vigorous stirring and left overnight for complete precipitation. The resultant solid product was filtered, washed with cold water, dried and recrystallized from ethanol<sup>10</sup>.

#### (ii) Synthesis of isoxazolines (II<sub>a-j</sub>)

Isoxazolines were prepared by reacting a mixture of purified chalcones (0.01 mol), hydroxylamine hydrochloride (0.01 mol) and a solution of sodium hydroxide (0.01 mol) in dry ethanol (50 ml) by refluxing for 6 hours on a water bath. After completion of the reaction, an excess of the solvent was removed by distillation and the resultant mass was poured into ice water with vigorous stirring. It was cooled overnight. The resultant solid product was filtered, washed with sufficient cold water, dried and purified by recrystallization from acetone<sup>10</sup>. (Scheme 3.1)



Scheme 3.1

Code no.	Ar	Abbreviated name	Code no.	Ar	Abbreviated name
II <sub>a</sub>	-H	ISO 1	II <sub>f</sub>		ISO 6
II <sub>b</sub>		ISO 2	II <sub>g</sub>		ISO 7
II <sub>c</sub>		ISO 3	II <sub>h</sub>		ISO 8
II <sub>d</sub>		ISO 4	II <sub>i</sub>		ISO 9
II <sub>e</sub>		ISO 5	II <sub>j</sub>		ISO 10

The synthesized compounds were characterized by FTIR spectra using IR Affinity 1 spectrometer (Shimadzu).

### 3.2.2 Corrosion monitoring techniques

#### Mild steel specimens and electrode

Cold rolled mild steel specimen of size 3 cm × 1 cm × 0.1 cm having composition 0.084% C, 0.369% Mn, 0.129% Si, 0.025% P, 0.027% S, 0.022% Cr, 0.011% Mo, 0.013% Ni and 99.32% of Fe were used for weight loss measurements. For electrochemical methods, a mild steel rod of same composition with an exposed area of 0.783 cm<sup>2</sup> was used. The specimens were polished with 1/0, 2/0, 3/0 and 4/0 grades of emery sheets and degreased with trichloroethylene and dried using a drier. The plates were kept in a desiccator to avoid the absorption of moisture.

#### Acid used

Analar grade sulphuric acid and double distilled water were used for preparing the solutions.

### **Corrosive solution**

1M H<sub>2</sub>SO<sub>4</sub> was prepared by dilution of analytical grade H<sub>2</sub>SO<sub>4</sub> with double distilled water. The concentration range of the inhibitors used was 0.5 mM - 10 mM in 1M sulphuric acid.

#### **3.2.2.1. Non-electrochemical measurements**

##### **1. Weight loss method**

The simplest and most accurate method for estimating the corrosion rate is weight loss analysis.

##### **Specimen preparation**

Mild steel specimens of size 3 cm x 1 cm x 0.1 cm were pickled in concentrated hydrochloric acid. The plates were washed, dried and polished successively using series of emery sheets of 1/0, 2/0, 3/0 and 4/0 grades to remove adhering impurities, degreased with trichloroethylene and dried using a drier. The plates were then kept in a dessicator to avoid the absorption of moisture.

##### **Experimental procedure**

The initial weight of the polished specimen was taken. The solutions were taken in 100 ml beakers and the specimens were suspended in triplicate into the solution using glass hooks. Care was taken to ensure the complete immersion of the specimen. After a period of three hours, the mild steel specimens were taken out, washed with distilled water, dried and weighed to the accuracy of four decimals. From the initial and final mass of the specimen, (*i.e.*, before and after immersion in the solution) the loss in weight was calculated. The experiment was repeated for various concentrations of the isoxazolines (II<sub>a-j</sub>).

In order to investigate the effect of temperature on the inhibitor performance, the above procedure was carried out in the different temperature range, 303 - 333 K with one hour immersion time, using a thermostat, with the inhibitor concentration of 10 mM.

##### **Calculations**

###### **(i) Evaluation of inhibition efficiency of the inhibitors**

From the initial and final weight of the specimen the percentage inhibition efficiency was determined.

$$\text{Inhibitor efficiency (\%)} = \frac{W_b - W_i}{W_b} \times 100$$

where,  $W_b$  = Weight loss without inhibitor;  $W_i$  = Weight loss with inhibitor.

### (ii) Evaluation of corrosion rate

The corrosion rate was calculated by measuring the loss in mass of specimen of known area to a particular environment (in the present investigation inside the electrolyte) for specified period using the formula,

$$\text{Corrosion rate (g cm}^{-2}\text{h}^{-1}\text{)} = \frac{534 \times \text{Weight loss in g}}{\text{Density} \times \text{Area (cm}^2\text{)} \times \text{Time in hrs}}$$

### (iii) Surface coverage ( $\theta$ )

The surface coverage ( $\theta$ ) was calculated using the following formula,

$$\text{Surface coverage (\theta)} = \frac{W_b - W_i}{W_b}$$

where,  $W_b$  = Weight loss without inhibitor;  $W_i$  = Weight loss with inhibitor.

### (iv) Calculation of activation energy ( $E_a$ )

The activation energy was calculated by graphical method by plotting  $\log$  (corrosion rate) vs.  $1000/T$  (K) with and without inhibitors at a concentration of 10 mM.  $E_a$  was calculated for all the inhibitors using the equation

$$E_a = -2.303 \times 8.314 \times \text{Slope (kJ)} \quad \longrightarrow \quad 3.1$$

### (v) Free energy of adsorption ( $\Delta G_{\text{ads}}^\circ$ )

The free energy of adsorption was calculated from the equilibrium constant of adsorption using the equation<sup>11</sup>

$$K = \frac{1}{55.5} \exp \left[ \frac{-\Delta G_{\text{ads}}^\circ}{RT} \right] \quad \longrightarrow \quad 3.2$$

where,

$$K = \frac{\theta}{C(1 - \theta)} \quad [\text{From Langmuir eqn}]$$

$\theta$  = Surface coverage of the inhibitor

$C$  = Concentration of the inhibitor in mM/100ml.

$$\Delta G_{\text{ads}}^\circ = -RT \ln (55.5K) \quad \longrightarrow \quad 3.3$$

### (vi) Kinetic parameters

The Transition state equation<sup>12</sup> was used to calculate thermodynamic parameters for the adsorption of inhibitors on mild steel surface. This equation shows the relationship between enthalpy of activation ( $\Delta H^\circ$ ) and entropy of activation ( $\Delta S^\circ$ ) and corrosion rate (CR) of mild steel as follows.

$$CR = RT \left[ \exp\left(\frac{\Delta S^\circ}{R}\right) \exp\left(\frac{-\Delta H^\circ}{RT}\right) \right] / Nh \quad \longrightarrow \quad 3.4$$

where R is the gas constant, T is the temperature, N is Avogadro's number and h is the Planck's constant. Rearranging and taking logarithm on both sides of equation 3.4

$$\log\left(\frac{CR}{T}\right) = \log\left(\frac{R}{Nh}\right) + \frac{\Delta S^\circ}{2.303R} - \frac{\Delta H^\circ}{2.303RT} \quad \longrightarrow \quad 3.5$$

A plot of  $\log(CR/T)$  vs.  $1/T$  should be a straight line with slope and intercept equal to  $-\frac{\Delta H^\circ}{2.303RT}$  and  $\log\left(\frac{R}{Nh}\right) + \frac{\Delta S^\circ}{2.303R}$  respectively.

## 2. Atomic absorption spectrophotometric studies

The weight loss can also be determined by the amount of metal dissolved in the solution using atomic absorption spectroscopy (AAS). Atomic Absorption Spectrophotometer (model GBC 908, Australia) was used for estimating the amount of dissolved iron in the corrosive solution. The polished mild steel specimens were immersed in 1M  $H_2SO_4$  containing various concentration of the isoxazolines (0.5 - 10 mM). After 3 hours of immersion, the amount of iron in the corrosive solution was determined using AAS. From the amount of dissolved iron, the inhibition efficiency was calculated.

$$\text{Inhibition efficiency (\%)} = \frac{B - A}{B} \times 100$$

where, A and B are the amount of dissolved iron in the presence and absence of inhibitor.

### 3.2.2.2 Electrochemical studies

Electrochemical techniques are now widely used to study the efficiency of the inhibitors. Since the electrochemical corrosion is the result of current flow between anodic and cathodic areas on a metal surface, the effect of the inhibitor will be to reduce this current.

## Electrode surface preparation

Mild steel rod of same composition embedded in Teflon with an exposed area of 0.783 cm<sup>2</sup> was polished using 1/0, 2/0, 3/0 and 4/0 grade emery papers and finally degreased using trichloroethylene and then placed in the test solution for 10 - 15 minutes before the measurement.

## Electrode cell assembly

Electrochemical measurements were carried out with a three electrode cell assembly. The working electrode was the mild steel rod. A saturated calomel electrode was used as the reference electrode and a rectangular platinum foil was used as counter or auxiliary electrode.

### 1. Electrochemical impedance measurements

The electrochemical impedance measurements were carried out for mild steel in acidic media using IVIUM (Compactstat Potentiostat/Galvanostat). After immersion of the specimen prior to the impedance measurement, a stabilization period of 30 minutes was observed for  $E_{oc}$  to attain a stable value. The impedance measurements were made at corrosion potentials over a frequency range of 10 kHz to 0.01 Hz with signal amplitude of 10 mV. The measurements were automatically controlled by IVIUM software and the impedance diagrams are given in Nyquist representation.

The real part ( $Z'$ ) and the imaginary part ( $Z''$ ) were measured at various frequencies. A plot of  $Z'$  vs.  $Z''$  were made. From the plot, the charge transfer resistance ( $R_{ct}$ ) and double layer capacitance ( $C_{dl}$ ) were calculated.

The charge transfer resistance ( $R_{ct}$ ) values were calculated from the difference in impedance at lower and higher frequencies. The double layer capacitance was obtained at the frequency  $f_{max}$  at which the imaginary component of the impedance is maximum ( $Z_{i,max}$ ) by the equation,

$$C_{dl} = \frac{1}{2\pi f_{max} R_{ct}} \longrightarrow 3.6$$

### Calculation

The Inhibition efficiency was calculated using the formula,



$$\text{Inhibition Efficiency (\%)} = \frac{R_{ct(\text{inh})} - R_{ct(\text{blank})}}{R_{ct(\text{inh})}} \times 100$$

where,  $R_{ct(\text{inh})}$  = charge transfer resistance in the presence of inhibitor;  $R_{ct(\text{blank})}$  = charge transfer resistance in the absence of inhibitor.

## 2. Polarization measurements

Polarization measurements were made after EIS studies in the same cell set up for a potential range of -200 mV to +200 mV with respect to open circuit potential at a sweep rate of 1mV/sec. The log of current and the corresponding potentials were fed out into the plotter and a potential E vs. log I plot was obtained. From the plot, the inhibitor efficiency, Tafel slopes, corrosion potentials and corrosion current were calculated using IVIUM software.

### Calculation

The inhibition efficiency was evaluated from the measured  $I_{\text{corr}}$  values using the following relationship,

$$\text{Inhibition Efficiency (\%)} = \frac{I_{\text{corr}(\text{blank})} - I_{\text{corr}(\text{inh})}}{I_{\text{corr}(\text{blank})}} \times 100$$

where  $I_{\text{corr}(\text{blank})}$  and  $I_{\text{corr}(\text{inh})}$  are the corrosion current density values without and with inhibitors respectively.

### 3.2.2.3 Surface examination study

#### 1. Scanning electron microscope-energy dispersive X-Ray spectroscopy (SEM-EDS)

Scanning electron microscopy (SEM) was used to study the surface morphology of the mild steel specimen. The surface morphology of the samples, after 3 hours immersion in 1M  $\text{H}_2\text{SO}_4$  solution in presence of selected concentrations of various inhibitors, was performed on Medzer biomedical research microscope. The presence of the inhibitor molecule on the mild steel surface was confirmed by EDS analysis.

#### 2. FTIR spectra of the corroded plates

Mild steel specimens were immersed in selected concentrations of the inhibitors for duration of 3 hours. After 3 hours, the specimens were taken out and dried. The surface of the metal specimen was analyzed by Fourier transform infrared spectra using FTIR-Affinity (Shimadzu).

### **3. XRD pattern of the corroded plates**

The corrosion products that were formed on the mild steel surface after its immersion for 3 hours in 1M H<sub>2</sub>SO<sub>4</sub> solution in the absence and presence of inhibitors were identified by an X-ray diffractometer (XRD; Bruker D8 Advance, Germany).

### **4. AFM of the corroded plates**

The surface morphology of the uninhibited and inhibited mild steel specimens was investigated by atomic force microscopy (AFM). For AFM analysis the mild steel specimens of size 3 cm x 1 cm x 0.1 cm were immersed in the test solution in the absence and presence of optimum concentration of the inhibitors for 3 hours at 303 K. After 3 hours the specimens were taken out from the solution, washed with distilled water, dried and used for AFM analysis. The AFM studies were carried out using Nova software by multimode scanning probe microscope (NTMDT, NTEGRA prima, Russia) with cantilever length, width and thickness 135, 30 and 2 μm respectively and 0.35 - 6.06 N/m force constant.

#### **3.2.3. Computational details**

##### **3.2.3.1 Quantum chemical studies**

B3LYP, a version of the DFT method that uses Becke's three parameter functional (B3) and includes a mixture of HF with DFT exchange terms associated with the gradient corrected correlation functional of Lee, Yang and Parr (LYP)<sup>13</sup>, was used to carry out quantum calculations. Then, full geometry optimization together with the vibrational analysis of the optimized structures of the inhibitor was carried out at the B3LYP/6-31G (d, p) level of theory using Gaussian 03 program package. The quantum chemical parameters were calculated for molecules in neutral as well as in the protonated form for comparison. It is well known that the phenomenon of electrochemical corrosion occurs in liquid phase. As a result, it was necessary to include the effect of a solvent in the computational calculations. In the Gaussian 03 program package, SCRF methods (Self-consistent reaction field) were used to perform calculations in aqueous solution. These methods model the solvent as a continuum of uniform dielectric constant and the solute is placed in the cavity within it.

There is no doubt that the recent progress in DFT has provided a very useful tool for understanding molecular properties and for describing the behaviour of atoms in molecules. DFT methods have become very popular in the last decade due to their accuracy and less computational time.

Density functional theory (DFT) using the functional B3LYP has been widely used in the description of the inhibitor metal surface mechanism and is also recommended for the study of chemical reactivity and selectivity of molecules. According to Koopman's theorem<sup>14, 15</sup> the ionization potential (I) and electron affinity (A) of the inhibitors are calculated using the following equations.

$$I = -E_{\text{HOMO}} \longrightarrow 3.7$$

$$I = -E_{\text{LUMO}} \longrightarrow 3.8$$

The higher HOMO energy corresponds to the more reactive molecule in the reactions with electrophiles, while lower LUMO energy is essential for molecular reactions with nucleophiles

Electronegativity( $\chi$ ) is the measure of the power of an electron or group of atoms to attract electrons towards itself<sup>16</sup> and is estimated using the following equation

$$\chi = \frac{I + A}{2} \longrightarrow 3.9$$

Global hardness ( $\eta$ ) measures the resistance of an atom to a charge transfer<sup>15</sup> and is obtained from the equation

$$\eta = \frac{I - A}{2} \longrightarrow 3.10$$

Global softness ( $\sigma$ ) describes the capacity of an atom or group of atoms to receive electrons<sup>15</sup> and is the inverse of global hardness. It is estimated by using the equation

$$\sigma = \frac{1}{\eta} \longrightarrow 3.11$$

Electronegativity, hardness and softness have proved to be very useful quantities in the chemical reactivity theory.

The global electrophilicity index ( $\omega$ ) was introduced by **Parr**<sup>17</sup> and is calculated using the electronic chemical potential and chemical hardness

$$\omega = \frac{\mu^2}{2\eta} \longrightarrow 3.12$$

According to the definition, this index measures the propensity of chemical species to accept electrons<sup>18</sup>. A good, more reactive, nucleophile is characterized by lower value of  $\omega$  and conversely a good electrophile is characterized by a high value of  $\omega$ . This new reactivity index measures the stabilization in energy when the system acquires an additional electronic charge  $\Delta N$  from the environment.

According to **Pearson** theory<sup>19</sup> the fraction of transferred electrons ( $\Delta N$ ) from the inhibitor molecule to the metallic atom can be calculated. For a reaction of two systems with different electronegativities (as a metallic surface and an inhibitor molecule) the following mechanism will take place: the electronic flow will occur from the molecule with the lower electronegativity toward that of higher value, until the chemical potentials are the same. For the calculations, the following formula was used

Thus, the fraction of electrons transferred from the inhibitor to metallic surface,  $\Delta N$ , is given by

$$\Delta N = \frac{\chi_{Fe} - \chi_{inh}}{2(\eta_{Fe} + \eta_{inh})} \longrightarrow 3.13$$

where,  $\chi_{Fe}$  and  $\chi_{inh}$  denote the absolute electronegativity of iron and inhibitor molecule;  $\eta_{Fe}$  and  $\eta_{inh}$  denote the absolute hardness of iron and the inhibitor molecule respectively. In order to calculate the fraction of electrons transferred, the theoretical value for the electronegativity of bulk iron was used  $\chi_{Fe}=7.0 \text{ eV}^{20}$  and a global hardness of  $\eta_{Fe} = 0$  by assuming that for a metallic bulk  $I = A^{21}$ . The difference in electro negativity drives the electron transfer and the sum of the hardness parameters acts as a resistance.

### 3.3 RESULTS

The present investigation aims to study the influence of isoxazolines on the corrosion of mild steel in 1M  $\text{H}_2\text{SO}_4$ . The results of non-electrochemical and electrochemical analysis carried out to find out the corrosion inhibition efficiency of isoxazolines are presented in this chapter. The amount of dissolved iron was also estimated by atomic absorption spectroscopic method.

The inhibitors were synthesized by condensing acetanilide with various aromatic aldehydes such as benzaldehyde, 3,4,5-trimethoxy benzaldehyde, vanillin, veratraldehyde, 2-nitrobenzaldehyde, p-dimethylamino benzaldehyde, anisaldehyde, 2-hydroxy naphthaldehyde, p-chlorobenzaldehyde and 4-hydroxy benzaldehyde. The

chalcones obtained were cyclised with nucleophilic reagent, hydroxylamine hydrochloride under reflux conditions to get isoxazolines. All the synthesized isoxazolines were characterized by IR spectra (Figs. 3.1 - 3.10). The IR spectra of isoxazolines ISO 1 - ISO 10 show bands around 3200 - 3300  $\text{cm}^{-1}$ , 1590 - 1660  $\text{cm}^{-1}$  and 1320 - 1390  $\text{cm}^{-1}$  characteristic of -NH, >C=N- and >C-O-N- stretching vibrations. IR spectra of ISO 3, ISO 8 and ISO 9 show broad bands around 3400  $\text{cm}^{-1}$  which may be attributed to a combination of -NH and -OH stretching vibrations. The weak bands in the region 2800 - 3100  $\text{cm}^{-1}$  are characteristic of >C-H stretching vibration in the aromatic ring. The bands around 1520 - 1558  $\text{cm}^{-1}$ , 1417 - 1468  $\text{cm}^{-1}$  are attributed to >C=C< stretching frequency of aromatic ring. The structure, physical properties and the significant FTIR bands of the synthesized isoxazolines are presented in Table 3.1.

### 3.3.1 Weight loss method

The gravimetric method is probably the most widely used method of inhibition assessment. The simplicity and reliability of the measurements offered by weight loss method is such that the technique forms the baseline method of measurement in many corrosion monitoring programmes.

Weight loss measurements were carried out at 303 K for different concentrations (0.5 mM – 10 mM) of isoxazolines after immersion in 1M  $\text{H}_2\text{SO}_4$  for 3 hours. From the weight loss, the inhibition efficiency (IE), corrosion rate (CR) and surface coverage ( $\theta$ ) were calculated and the results are presented in Table 3.2. The values in Table 3.2 reveal that the isoxazolines efficiently inhibit the corrosion of mild steel in 1M  $\text{H}_2\text{SO}_4$ . The corrosion rate decreased considerably with an increase in the concentration of the inhibitor. This is due to the presence of heteroatoms like nitrogen, oxygen and aromatic rings. The extent of inhibition depends upon the nature and mode of adsorption of inhibitor on the metal surface. The adsorption is assumed to be a quasi substitution process between water molecules on the surface and the inhibitor. The isoxazolines are adsorbed on the metal surface by flat orientation. Increase in percentage inhibition efficiency with an increase in the concentration of the inhibitors, suggest that the number of molecules adsorbed increased over the mild steel surface blocking the active sites of acid attack and thereby protecting the metal from corrosion. At highest concentration of 10 mM of isoxazolines, the percentage inhibition efficiency was above 80% which

confirmed that isoxazolines were very effective inhibitors. The high percentage inhibition efficiency of isoxazolines may be attributed to the presence of a number of anchoring sites namely –NH, lone pair of electrons on the ring N, O and the  $\pi$ -bonds of the benzene and isoxazoline rings.

To investigate the mechanism of inhibition and to calculate the thermodynamic parameters for the corrosion process, weight loss measurements were carried out at varying temperatures ranging from 303 - 333 K with 10 mM of the inhibitor. The weight loss recorded, corrosion rate and percentage inhibition efficiency are given in Table 3.3. Inhibition efficiency decreased with increase in temperature.

The activation energy  $E_a$  was calculated from the slope obtained by plotting log corrosion rate vs.  $1000/T$  (Fig. 3.11, Table 3.4). The values of  $E_a$  in the presence of the isoxazolines are higher than those in the uninhibited acid solution ( $48.45 \text{ kJ mol}^{-1}$ ). This is because the organic compounds have reaction centers that can block the active sites for corrosion resulting in an increase in activation energy.

### 3.3.2 Electrochemical impedance spectroscopic method

Impedance measurement is a veritable tool and has been widely used in investigating the corrosion inhibition processes. It provides information on both the resistive and capacitive behaviour at the interface and makes it possible to evaluate the performance of the tested compounds as possible inhibitors against metals.

Nyquist plots of the isoxazolines (ISO 1 – ISO 10) in 1M  $\text{H}_2\text{SO}_4$  in the absence and presence of various concentrations are shown in Figs. 3.18 a-j. The impedance spectra shows a single semicircle and the diameter of the semicircle increases with increasing inhibitor concentration. The diagrams exhibit one capacitive loop at high frequency which is attributed to charge transfer of the corrosion process<sup>22</sup>. Various parameters such as charge transfer resistance ( $R_{ct}$ ), double layer capacitance ( $C_{dl}$ ) and inhibition efficiency obtained from impedance measurements are presented in Table 3.10.  $R_t$  values were calculated from the difference in impedance at lower and higher frequencies as suggested by **Tsuru *et al.***,<sup>23</sup>  $C_{dl}$  values were calculated from the frequency at which the imaginary component of impedance was maximum ( $f_{max}$ ) using the relation,

$$C_{dl} = \frac{1}{2\pi f_{max} R_{ct}} \longrightarrow 3.14$$

The double layer capacitance values are found to decrease with the increase in inhibitor concentration. The inhibition efficiency values are found to increase with increase in the concentration of the inhibitors.

### 3.3.3 Potentiodynamic polarization method

Polarization measurements were carried out in order to gain knowledge concerning the kinetics of the cathodic and anodic reactions. The polarization behaviour of mild steel in 1M H<sub>2</sub>SO<sub>4</sub> containing different concentrations of isoxazolines (ISO 1- ISO 10) are shown in Figs. 3.19 a-j. Electrochemical parameters such as I<sub>corr</sub>, E<sub>corr</sub>, b<sub>a</sub> and b<sub>c</sub> obtained from Tafel plots extracted from these curves are given in Table 3.11. The corrosion current density (I<sub>corr</sub>) values were obtained by extrapolating both the cathodic and anodic Tafel slopes to the corrosion potential (E<sub>corr</sub>). I<sub>corr</sub> values decreased and percentage inhibition efficiency increased with increase in inhibitor concentration.

## 3.4 DISCUSSION

### 3.4.1 Mechanism of adsorption of organic compounds on the mild steel surface

Adsorption studies with different types of metal surface using organic compounds containing aromatic rings reveal that these compounds in general adsorb through a flat orientation on the metal surface. Further there seems to be a definite correlation between the potential of zero charge of the metal surface and adsorption of organic compounds on them.

The adsorption of organic compounds on iron surface has to be dealt with utmost care due to the following peculiarities of iron group of metals.

i. The energy of adsorption -  $\Delta G^{\circ}_{\text{ads}}$  of water molecule is higher on metals of high hydrogen overvoltage (such as Hg) and on silver and copper. It is because of this hydrophilic nature of iron surface benzyl alcohol is not adsorbed to any appreciable extent on iron<sup>24</sup>.

ii. The partially filled d-orbitals of iron group of metals have a significant influence on the mechanism of adsorption of organic compounds.

iii. The surfaces of iron, cobalt and nickel are oxidized fairly easily in air or in aqueous solutions. The presence of an oxide film alters the adsorption activity of the electrode surface substantially.

iv. In contrast to the metals of high hydrogen overvoltage, a potential region in which the iron group of metals behaved as ideally polarized electrodes cannot be well defined.

The above peculiarities of the iron group of metals lead sometimes to contradictory experimental data for the same study and render the interpretation of the observed data extremely difficult.

Due to the above peculiarities, several factors influence the adsorption of organic compounds on the metals of the iron group.

i. Adsorption of organic compounds on iron group of metals is found to depend on the potential and the position of zero charge in a given medium. To quote, according to **Bockris *et al.***,<sup>25, 26</sup> the shift of the potential of maximum adsorption ( $\phi_m$ ) of iron and nickel in the negative region relative to PZC ( $\phi_n = -0.47$  vs. NHE) is due to the difference in the adsorption energy of water dipoles at positive and negative charges of the metal surface. However, **Damaskin *et al.***, differ from this view and opine that the dependence of adsorption of organic compounds on the potential is less pronounced with metals of the iron group than with Hg, probably due to the high energy of adsorption ( $-\Delta G^\circ_{\text{ads}}$ ) of organic compounds than the adsorption energy of water molecules<sup>27</sup>. Probably, the difference in the opinion of several authors on the true position of PZC of iron group of metals that might have led **Damaskin *et al.***, to make such a conclusion.

ii. The co-adsorption of anions of the medium with the organic substances seem to influence the adsorption capabilities of these compounds<sup>28, 29</sup> and this has been attributed to (a) the change of surface charge by a shift in PZC through chemisorption of anions and (b) the rendering of the surface hydrophobic in the presence of anions.

iii. The adsorption of organic compounds on iron surface has also been found to be influenced by the structure of the inhibitor molecules and there seems to be a definite correlation between their absorbability and inhibiting action<sup>30-35</sup>. For instance, the derivatives of ethylene<sup>36</sup> and especially of acetylene<sup>37, 38</sup> series have higher adsorption activity owing to interaction of  $\pi$ -electrons with the surface atoms of the adsorbent.



iv. The adsorbed reaction products and intermediates also seem to influence the adsorption of organic compounds on the surface of the iron group of metals. It is suggested that the presence of adsorbed particles (OH, H), saturate the free valence bonds of the surface metal atoms and lower the energy of adsorption of organic compounds leading to their low adsorbabilities<sup>39</sup>. Many investigators consider that low adsorbability of organic compounds is due to the presence of oxides on the metal surface, which intensify its hydrophobic properties. On the other hand organic compounds with iron ions are adsorbed well as on iron<sup>40, 41</sup>.

v. Adsorption of a number of organic compounds on metals of iron group is accompanied by chemical changes of the adsorbed molecules. Appearance of new species on the electrode surface alters the inhibiting influence of organic compounds on electrode reactions<sup>42, 43</sup> (secondary inhibition).

From the above discussion, the following conclusions can be drawn on the mechanism of adsorption of organic compounds on metal surfaces.

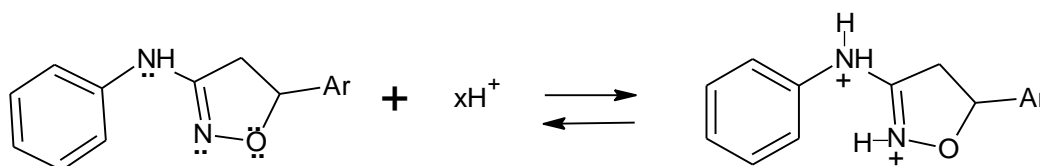
- i. Irrespective of the nature of the metal surface, whether it belongs to the metals of high, medium or low hydrogen overvoltage, organic compounds with aromatic rings prefer to adsorb through the flat orientation of the entire molecule including its aromatic ring on the metal surface. This is because, in the flat orientation, there is maximum adsorption due to the interaction between  $\pi$ -electrons of the ring as well as the unshared electron pairs of the hetero atoms with the metal surface.
- ii. Despite the fact that iron is highly hydrophilic due to the large  $-\Delta G^{\circ}_{\text{ads}}$  for water and despite the fact that surface charge of the metal with reference to PZC is unfavourable to the adsorption of organic compounds in a given medium, organic compounds with aromatic rings are strongly adsorbed on iron surface. This is evidently due to the predominance of  $\pi$ -electron interaction over the potential and surface charge factors.
- iii. Adsorption of anions from the aggressive medium or from the added salts in general induces co-adsorption and thereby synergistically influences the adsorption of organic compounds on iron surface.
- iv. The adsorbed reaction products may either enhance or decrease the magnitude of adsorption depending on the nature of the adsorption reaction product.

### 3.4.2 Adsorption of isoxazolines on mild steel surface

As far as the inhibition process is concerned, it is generally assumed that adsorption of the inhibitor at the metal solution interface is the first step in the action mechanism of the inhibitors in aggressive acid media. Four types of adsorption may take place during inhibition involving organic inhibitor at the metal solution interface.

- (i) Electrostatic attraction between charged molecules and the charged metal.
- (ii) Interaction of unshared electron pairs in the molecule with the metal.
- (iii) Interaction of  $\pi$  electrons of the aromatic and isoxazoline rings with the metal.
- (iv) A combination of the above<sup>44</sup>

In the present work, isoxazolines contain two nitrogen atoms and one oxygen atom which can be protonated in acid medium. Thus they become cations, existing in equilibrium with the corresponding molecular form.



In the presence of  $\text{H}_2\text{SO}_4$ , the negatively charged  $\text{SO}_4^{2-}$  would attach to the positively charged metal surface, thereby the protonated ion may also get adsorbed onto the metal surface<sup>45, 46</sup> (**Fig. i**). Since an equilibrium exist between non-protonated and protonated species, there is also a possibility for the interaction of the lone pair of electrons on N and O atoms of the non-protonated molecules with the metal surface (**Fig. ii**). The  $\pi$ -electrons of the aromatic rings and isoxazoline ring may also interact with the metal surface (**Fig. iii**). Hence, it can be concluded that the isoxazoline molecules get adsorbed on the mild steel surface based on the above three mechanisms.

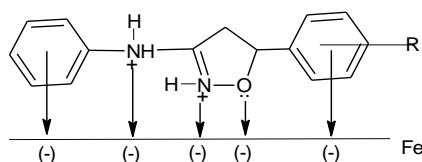


**Fig. i**

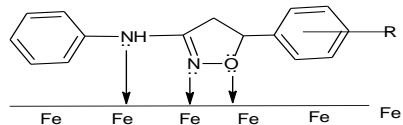


**Fig. ii**

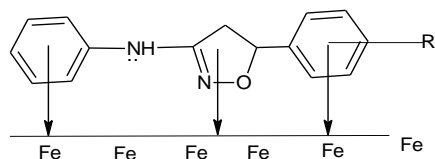


**Fig. iii**

**Fig. i, ii and iii: represents schematic diagram for adsorption of isoxazolines on mild steel surface**

### 3.4.3 Nature of adsorption- Effect of temperature on inhibition efficiency

One of the most perplexing questions to be answered in the current Chapter is whether the adsorption is purely physical or chemical in nature.

Two main types of adsorption may be distinguished. In the first type the forces are of physical nature and the adsorption is relatively weak. The forces in this type of adsorption are known as van der Waals forces or dispersion forces and this type of adsorption is called van der Waals adsorption, physical adsorption or physisorption. The heat evolved in this adsorption is less than  $20 \text{ kJ mol}^{-1}$ . In the second type of adsorption, the adsorbed molecules are held to the surface by covalent forces. The heat evolved for this type of adsorption known as chemisorption is usually comparable to that evolved in chemical bonding, namely  $300 - 500 \text{ kJ mol}^{-1}$ .

While deriving the mechanism of adsorption in Sec. 3.4.1, it was concluded that three adsorption mechanisms might have contributed to the actual mechanism of adsorption. The first is one in which the protonated cationic inhibitor molecules electrostatically interact with the negatively charged metal surface. In the second mechanism, the unpaired electrons of the N-atoms involve in a co-ordinate covalent type of bond with the Fe atoms through their vacant d-orbitals. In the third mechanism, the  $\pi$ -electrons of the aromatic ring and  $>\text{C}=\text{N}$  - group interact with the vacant d-orbitals of Fe atoms at active centres. While the first mechanism is physical type, the remaining two are chemisorption mechanisms. Hence, it seems that the adsorption is not purely physical

or chemical in nature. It can only be interpreted, which predominates over the other. This can be achieved through the study of temperature effects on corrosion and corrosion inhibition.

The effect of temperature on the inhibited acid-metal reaction is highly complex because many changes occur on the metal surface, such as rapid etching and desorption of the inhibitor and the inhibitor itself, but in some cases it may undergo decomposition and/or rearrangement. However, it provides the ability of calculating many thermodynamic functions for the inhibition and/or the adsorption processes which contribute in determining the type of adsorption of the studied inhibitors<sup>47, 48</sup>.

Temperature has a great effect on the rate of metal electrochemical corrosion. Some authors (**Popova, Obi-Egbedi and Obot**)<sup>49, 50</sup> opined that for corrosion in a neutral solution (oxygen depolarization) the increase in temperature has a favourable effect on the overpotential of oxygen depolarization and the rate of oxygen diffusion but leads to a decrease of oxygen solubility, whereas for corrosion in acidic medium (hydrogen depolarization), the corrosion rate increases exponentially with temperature increase because the hydrogen evolution overpotential decreases. Effect of temperature on the corrosion and inhibition process of mild steel in 1M H<sub>2</sub>SO<sub>4</sub> in the absence and presence of optimum concentration (10 mM) of the isoxazolines after 1 hour of immersion was studied at 303 - 333 K using weight loss measurements.

**(i) Activation parameters for corrosion process**

The corrosion rates evaluated at different temperatures in the absence and presence of isoxazolines were used to calculate the activation energy of the metal dissolution. Most of the authors used Arrhenius equation to calculate the apparent activation energy of corrosion process<sup>51,52,53</sup> of mild steel in acid medium,

$$\log CR = \frac{-E_a}{2.303RT} + \log \lambda \quad \longrightarrow \quad 3.15$$

where CR is the corrosion rate, E<sub>a</sub> is the the apparent activation energy of the mild steel dissolution, R is the molar gas constant, T is the absolute temperature and A is the Arrhenius pre-exponential factor. Using equation 3.15 and from a plot of log CR vs. 1000/T (Fig. 3.11) the values of E<sub>a</sub> and λ at 10 mM concentration of the isoxazolines were computed from slopes and intercepts respectively and the values are

given in Table 3.4. The data showed that the activation energy for the corrosion of mild steel in 1M H<sub>2</sub>SO<sub>4</sub> in the presence of inhibitor is higher than that of free acid. This indicated that the used inhibitors considerably increase the activation energy of the corrosion process due to their adsorption onto the metal surface<sup>54, 55</sup>. In the literature, lower activation energy value for corrosion process in the presence of the inhibitor is attributed to its chemisorption, while the higher value is associated with its physical adsorption<sup>56</sup>. The increased activation energy in the presence of the inhibitor suggest that adsorbed isoxazolines create a physical barrier to charge and mass transfer, leading to reduction in corrosion rate<sup>57</sup>.

The large increase in the activation energy of the corrosion process in the presence of the inhibitor may be attributed to the slow rate of inhibitor adsorption on the metal surface at higher temperature as reported by **Hoar** and **Holiday**<sup>58</sup>. But, **Riggs** and **Hurd**<sup>59</sup> explained that, the increase in the activation energy of corrosion at higher levels of inhibition arises from a shift of the net corrosion reaction from that on the uncovered part on the metal surface to the covered one. **Schmid** and **Huang**<sup>60</sup> and **Hegazy**<sup>61</sup> found that, the organic molecules inhibit both the anodic and cathodic partial reactions on the electrode surface and a parallel reaction takes place on the covered area, but the reaction rate on the covered area is substantially less than on the uncovered area. This is in agreement with the results of this work as represented in Table 3.4.

The values of enthalpy of activation  $\Delta H^\circ$  and entropy of activation  $\Delta S^\circ$  were obtained from the transition state equation<sup>62</sup>

$$C_R = \frac{RT}{Nh} \exp\left(\frac{\Delta S^\circ}{R}\right) \exp\left(-\frac{\Delta H^\circ}{RT}\right) \quad \longrightarrow \quad 3.16$$

where h is the Planck's constant, N is the Avogadro number, R is the molar gas constant, T is the absolute temperature,  $\Delta H^\circ$  is the enthalpy of activation and  $\Delta S^\circ$  is the entropy of activation. A plot of  $\log CR/T$  as a function of  $1000/T$  (Fig. 3.12) was made for mild steel corrosion in 1M H<sub>2</sub>SO<sub>4</sub> in the presence and absence of isoxazolines. Straight lines were obtained with slope  $-\Delta H^\circ/2.303R$  and intercept  $[\log(R/Nh) + (\Delta S^\circ/2.303R)]$  from which the activation thermodynamic parameters  $\Delta H^\circ$  and  $\Delta S^\circ$  were computed and listed in Table 3.4. Examination of these data reveal that the  $\Delta H^\circ$  values for dissolution reaction of mild steel in 1M H<sub>2</sub>SO<sub>4</sub> in the presence of the inhibitors are higher

(58.53 - 74.30 kJ mol<sup>-1</sup>) than that in the blank (45.81 kJ mol<sup>-1</sup>) indicating higher protection efficiency. This may be attributed to the presence of energy barrier for the reaction; hence the process of adsorption of inhibitor leads to rise in enthalpy of the corrosion process.

The positive sign of the enthalpy reflects the endothermic nature of the mild steel dissolution process<sup>49, 63</sup>. The negative values of  $\Delta S^\circ$  for all the studied inhibitors implies that the formation of the activated complex in the rate determining step represents an association rather than a dissociation step, meaning that a decrease in disordering takes place during the course of the transition from reactants to the activated complex<sup>64</sup>.

The change in free energy of activation  $\Delta G^\circ$  for the corrosion process can be calculated at each temperature by applying the thermodynamic relation,

$$\Delta G^\circ = \Delta H^\circ - T \Delta S^\circ \quad \longrightarrow \quad 3.17$$

The obtained values of  $\Delta G^\circ$  are listed in Table 3.4. The values were positive and increased with increase in temperature. With an increase in temperature the spontaneity of the corrosion process increases indicating the solubility of the activated complex at higher temperatures.

## **(ii) Adsorption isotherm and adsorption parameters**

The extent of corrosion inhibition depends on the surface conditions and the mode of adsorption of the inhibitors<sup>65</sup>. Under the assumptions that the corrosion of the covered parts of the surface is equal to zero and that corrosion takes place only on the uncovered parts of the surface (*i.e.*, inhibitor efficiency is mainly due to the blocking effect of the adsorbed species), the degree of surface coverage ' $\theta$ ' has been estimated from the chemical and electrochemical techniques employed in this study as follows:  $\theta = \text{IE} (\%) / 100$  (assuming a direct relationship between surface coverage and inhibition efficiency)<sup>65-68</sup>. The adsorption on the corroding surfaces never reaches the real equilibrium and tends to reach an adsorption steady state. However, when the corrosion rate is sufficiently small, the adsorption steady state has a tendency to become a quasi-equilibrium state. In this case, it is reasonable to consider the quasi-equilibrium adsorption in thermodynamic way using the appropriate equilibrium adsorption isotherms<sup>69</sup>.

Adsorption isotherms are very important in determining the mechanism of organoelectrochemical reaction<sup>70-72</sup>. The most frequently used isotherms are Langmuir, Frumkin, Hill de-Boar, Parsons, Temkin, Flory Huggin, Freundlich, Dhar-Flory-Huggin, kinetic/thermodynamic model of **El-Awady *et al.***, and **Bockris Swinkels**. All these isotherms are expressed in a general form

$$f(\theta, x) \exp(-2a\theta) = K_{\text{ads}} C \quad \longrightarrow \quad 3.18$$

where  $f(\theta, x)$  is configurational factor which depends upon the physical model and the assumptions underlying the derivation of the isotherm,  $\theta$  is the surface coverage,  $C$  is the inhibitor concentration in the electrolyte, 'x' is the size factor ratio, 'a' is the molecular interaction parameter and 'K' is the equilibrium constant of the adsorption process.

Basic information on the interaction between the inhibitor and the mild steel surface can be provided by the adsorption isotherm. In order to obtain the isotherm, the linear relation between the values of  $\theta$  and the inhibitor concentration ( $C_{\text{inh}}$ ) must be found. Attempts were made to fit  $\theta$  values to the thermodynamic-kinetic model of Flory-Huggins, Temkin and Langmuir isotherms and the correlation coefficient ( $R^2$ ) values were used to determine the best fit isotherm. In the present work, Langmuir, Flory-Huggins and Temkin adsorption isotherms were applied to explain the adsorption process of isoxazolines on the mild steel surface.

The surface coverage values for isoxazolines were fitted into the Temkin adsorption isotherm model, which has the form:

$$\exp(-2a\theta) = KC \quad \longrightarrow \quad 3.19$$

where 'a' is molecular interaction parameter, ' $\theta$ ' is the degree of surface coverage, 'K' is equilibrium constant of adsorption process and 'C' is the concentration of the inhibitor. The plot of surface coverage as a function of logarithm of inhibitor concentration is shown in Fig. 3.13 (Temkin adsorption isotherm). From the plot and Table 3.5, it is clear that  $R^2$  values are less than 0.99 indicating that the experimental data do not fit into the Temkin adsorption isotherm.

Then attempts were made to fit the adsorption data into Flory-Huggins adsorption isotherm. The Flory-Huggins adsorption isotherm is given by the following equation

$$\log(\theta / C) = \log K + x \log(1 - \theta) \quad \longrightarrow \quad 3.20$$

It is evident from Fig. 3.14 that the experimental data do not fit well into Flory-Huggins

adsorption isotherm. This is further supported by the observation that the  $R^2$  value is less than unity as shown in Table 3.5.

Langmuir adsorption isotherm was found to be suitable for the experimental findings. The Langmuir isotherm is based on the assumption that all adsorption sites are equivalent and that particle binding occurs independently from nearby sites whether occupied or not. By far the best fit is obtained with Langmuir isotherm. According to this isotherm,  $\theta$  is related to  $C_{inh}$  by the following equation.

$$\frac{C}{\theta} = \frac{1}{K_{ads}} + C \quad \longrightarrow \quad 3.21$$

where,

$$K_{ads} = \frac{1}{55.5} \exp\left(-\frac{\Delta G_{ads}^{\circ}}{RT}\right) \quad \longrightarrow \quad 3.22$$

where 55.5 represents the molar concentration of water in solution ( $\text{mol L}^{-1}$ ),  $R$  is the universal gas constant,  $T$  is the absolute temperature,  $C$  is the inhibitor concentration,  $K_{ads}$  is the adsorption equilibrium constant and  $\Delta G_{ads}^{\circ}$  is the standard free energy of adsorption. The values of regression coefficients ( $R^2$ ) confirmed the validity of this approach. The straight line was obtained for the plot of  $C/\theta$  versus  $C$  (Fig. 3.15) with slope close to unity. This suggests that the adsorption of the isoxazolines obeyed the Langmuir's adsorption isotherm model. A straight line was obtained suggesting that the adsorbed inhibitor molecules form monolayer on the mild steel surface and there is no interaction among the adsorbed inhibitor molecules<sup>73</sup>. The  $K_{ads}$  values can be calculated from the intercept lines on the  $C_{inh}/\theta$ -axis. This is related to the standard free energy of adsorption ( $\Delta G_{ads}^{\circ}$ ) with the following equation<sup>74</sup> and the calculated values are tabulated in Table 3.6.

$$\Delta G_{ads}^{\circ} = -RT \ln(55.5K) \quad \longrightarrow \quad 3.23$$

where,  $R$  is the gas constant and  $T$  is the absolute temperature. The constant value of 55.5 is the concentration of water in solution in  $\text{mol dm}^{-3}$ . The negative value of  $\Delta G_{ads}^{\circ}$  ensure the spontaneity of the adsorption process and stability of the adsorbed layer on the mild steel surface. It is well known that the values of  $\Delta G_{ads}^{\circ}$  of order of  $20 \text{ kJ mol}^{-1}$  or lower is consistent with the electrostatic interaction between the charged molecules and the charged metal and indicate a physisorption; while those of order of  $40 \text{ kJ mol}^{-1}$  involve



charge sharing or transfer from the inhibitor molecules to the metal surface to form a co-ordinate bond (chemisorptions). The calculated  $\Delta G_{ads}^\circ$  values for isoxazolines were found between -21.72 to -29.79 kJ mol<sup>-1</sup> confirmed the mixed mode of adsorption.

How do the observed data in the present studies conform to Langmuir isotherm instead of Temkin or Frumkin as observed in most cases for organic compounds? The most probable solution to this fascinating question can be obtained if we consider the expressions for the three isotherms.

$$\text{Temkin} \quad \theta = \frac{1}{f} [B_{\max} C] \quad \longrightarrow \quad 3.24$$

Where  $f$  = heterogeneity factor for metal surface;  $B_{\max} = \exp^{(-\Delta G_{ads}/2RT)}$

$$\text{Frumkin} \quad BC = \frac{\theta}{1-\theta} \exp(-2a\theta) \quad \longrightarrow \quad 3.25$$

$a$  = interaction parameter for adsorbed species,

$a > 0$  means attraction and  $a < 0$  means repulsion

$$\text{Langmuir} \quad BC = \frac{\theta}{1-\theta} \quad \longrightarrow \quad 3.26$$

It has been suggested by **Damaskin *et al.***,<sup>75</sup> that on surfaces of high heterogeneity like iron surface, the conformity of observed data to Langmuir equation is brought about by the action of two mutually compensating factors. According to **Damaskin *et al.***, while on one hand the free energy of adsorption decreases with increasing surface coverage, on the other, it increases due to attractive forces between adsorbed molecules, that is mutual compensation of the effects of the exponential terms in the Temkin isotherm (equation 3.24) and the Frumkin isotherm (equation 3.25) occurs. This leads to the transformation of these two isotherms into Langmuir isotherm (equation 3.26). As a result the observed data will conform to Langmuir isotherm. Hence, most probably for the above reason the observed adsorption data for all the isoxazolines conform to Langmuir adsorption isotherm.

Moreover, the Langmuir adsorption isotherm can be expressed in terms of a dimensionless separation factor,  $R_L$ <sup>76</sup>, which describes the type of isotherm and is defined by:

$$R_L = \frac{1}{1 + K_{ads}C} \quad \longrightarrow \quad 3.27$$

A small  $R_L$  value indicates a highly favorable adsorption. If  $R_L > 1$ , unfavorable;  $R_L = 1$ , linear;  $0 < R_L < 1$ , favorable; and if  $R_L=0$ , irreversible. Table 3.7 gives the estimated values of  $R_L$  for isoxazoline compounds at different concentrations. It was found that all  $R_L$  values are less than unity, confirming that the adsorption processes are favourable.

### (iii) Thermodynamic parameters

Thermodynamic parameters are considered very important in carrying out the studies about the adsorption of inhibitors on the metal surface. The corrosion inhibition of isoxazolines for the surface of mild steel could be well explained by using thermodynamic model. The heat of adsorption, the free energy of adsorption and the entropy of adsorption were calculated to explain the inhibition action of isoxazolines. Thermodynamic parameters such as enthalpy of adsorption  $\Delta H_{ads}^\circ$  and entropy of adsorption  $\Delta S_{ads}^\circ$  can be deduced from integrated version of the Van't Hoff equation expressed in the following equation<sup>77</sup>

$$\ln K_{ads} = -\frac{\Delta H_{ads}^\circ}{RT} + \frac{\Delta S_{ads}^\circ}{T} + \ln \frac{1}{55.5} \quad \longrightarrow \quad 3.28$$

Fig. 3.16 shows the plot of  $\ln K_{ads}$  vs.  $1/T$  for mild steel dissolution in 1M  $H_2SO_4$  which gives straight lines with slope  $(-\Delta H_{ads}^\circ/2.303R)$  and intercept  $(\Delta S_{ads}^\circ/R + \ln 1/55.5)$ . The calculated values of  $\Delta H_{ads}^\circ$  and  $\Delta S_{ads}^\circ$  using the Van't Hoff equation are compiled in Table 3.8. The heat of adsorption can be considered as the standard adsorption heat under the experimental conditions<sup>78, 79</sup>. The negative values of heat of adsorption indicate that the adsorption of all the isoxazolines is an exothermic process. It is reported that an exothermic adsorption process resembles either physisorption or chemisorption, while the endothermic adsorption process is applicable to chemisorption<sup>80</sup>. This is due to desorption of adsorbed inhibitor molecules from the mild steel surface at higher temperatures.

The enthalpy of adsorption  $\Delta H_{ads}^\circ$  found by the Van't Hoff equation, may be evaluated by the Gibbs–Helmholtz equation, which is defined as follows:

$$\frac{\partial(\Delta G_{ads}^\circ/T)}{\partial T} = \frac{-\Delta H_{ads}^\circ}{T^2} \quad \longrightarrow \quad 3.29$$

This equation can be arranged to give

$$\frac{\Delta G_{\text{ads}}^{\circ}}{T} = \frac{\Delta H_{\text{ads}}^{\circ}}{T} + K \quad \longrightarrow \quad 3.30$$

The variation of  $\Delta G_{\text{ads}}^{\circ}/T$  with  $1/T$  gives a straight line with slope equal to  $\Delta H_{\text{ads}}^{\circ}$  (Fig. 3.17). The value of the enthalpy of adsorption  $\Delta H_{\text{ads}}^{\circ}$  found by the two methods such as Van't Hoff and Gibbs–Helmholtz relations are in good agreement<sup>81</sup>

#### 3.4.4 Atomic absorption spectrophotometric studies

The amount of iron dissolved in the presence of isoxazolines when mild steel specimens are exposed to 1M H<sub>2</sub>SO<sub>4</sub> were calculated and presented in Table 3.9. It has been found that the amount of dissolved iron in the corrodent solution decreases with increase in concentration of the inhibitors and there is good agreement between values of percentage inhibition efficiency calculated from weight loss and AAS technique.

#### 3.4.5 Electrochemical behaviour of inhibition

In the present thesis only two electrochemical techniques *viz.*, electrochemical impedance spectroscopy and potentiodynamic polarization have been employed for the investigation of corrosion and its inhibition and hence the results from only these two techniques have been discussed in this part.

##### (i) Impedance behaviour of inhibition

The results of the electrochemical impedance spectroscopic measurements could be better interpreted by taking into consideration the following theoretical aspects. A simple electrode reaction such as metal deposition or metal dissolution can be represented by an equivalent circuit, named as Randles equivalent circuit with various components as shown in (Fig. iv). This circuit represents the cell impedance under the most simplified circumstances, with which the various components of the cell have been derived by **Randles**<sup>82</sup>, **Delahay**<sup>83</sup> and **Sluyters *et al.***<sup>84</sup>

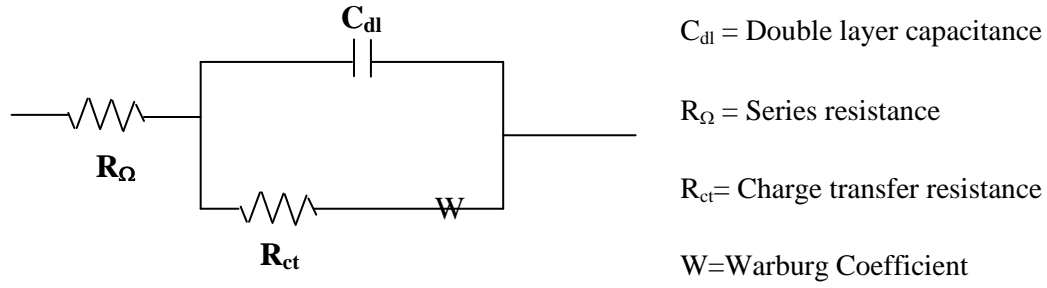


**Fig. iv: Equivalent circuit of electrode impedance**

By adopting complex plane analysis for the total cell impedance  $Z$ , *Sluyters et al.*, have resolved it into real and imaginary components as

$$Z' = R_{\Omega} + \frac{R_{ct} + \sigma \omega^{-1/2}}{(\sigma \omega^{1/2} C_{dl} + 1)^2 + \omega^2 C_{dl}^2 (R_{ct} + \sigma \omega^{-1/2})^2} \longrightarrow 3.31$$

$$Z'' = R_{\Omega} + \frac{\omega C_{dl} (R_{ct} + \sigma \omega^{-1/2})^2 + \sigma^2 C_{dl} + \sigma \omega^{-1/2}}{(\sigma \omega^{1/2} C_{dl} + 1)^2 + \omega^2 C_{dl}^2 (R_{ct} + \sigma \omega^{-1/2})^2} \longrightarrow 3.32$$

The various components of cell impedance, viz.,  $R_{ct}$ ,  $\sigma$  (Warburg coefficient),  $C_{dl}$  and  $R_{\Omega}$  can be evaluated by taking two extreme types of electrode reaction.

**Type: 1** For a purely diffusion controlled reaction (concentration polarized)

For such a reaction at low frequency,

$$Z' = R_{\Omega} + R_{ct} + \sigma \omega^{-1/2} \longrightarrow 3.33$$

and  $Z'' = [\sigma \omega^{-1/2} + 2\sigma^2 C_{dl}] \longrightarrow 3.34$

For such a reaction a plot of  $Z''$  vs.  $Z'$  leads to a straight line with a slope of  $45^\circ$  (Fig. v).

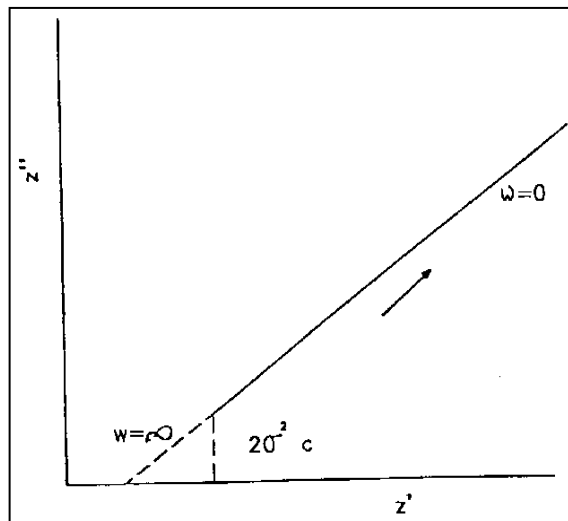


**Fig. v: Low frequency electrode impedance**

**Type 2:** For a purely activation controlled reaction

In the case of an irreversible electrode process such as corrosion and at high frequencies, the process is activation polarization controlled. The concentration polarization,  $\sigma$  can be neglected and the equivalent circuit to a great approximation is modified as in (Fig. vi).

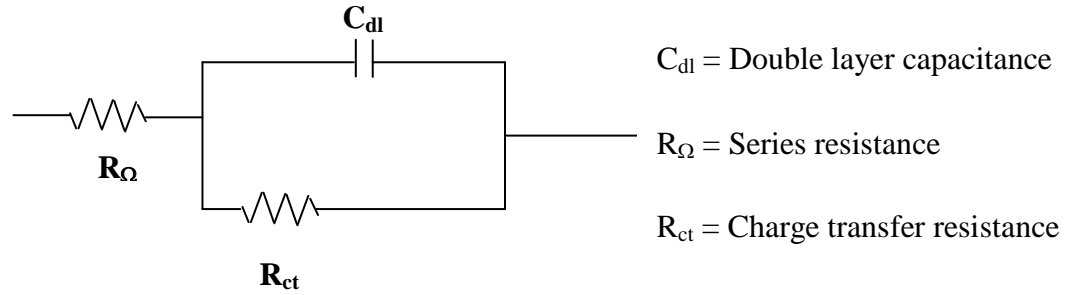


**Fig. vi: Modified equivalent circuit of electrode impedance**

Consequently the real and imaginary components of cell impedance becomes

$$Z' = R_{\Omega} + R_{ct} / (1 + \omega^2 C_{dl}^2 R_{ct}^2) \quad \longrightarrow \quad 3.35$$

$$Z'' = \omega C_{dl} R_{ct}^2 / (1 + \omega^2 C_{dl}^2 R_{ct}^2) \quad \longrightarrow \quad 3.36$$

Elimination of  $\omega$  is performed by inserting  $\omega = Z'' / (Z' - R_{\Omega}) R_{ct} C_{dl}$  into equation 3.36 and rearranging to

$$\left[ Z' - R_{\Omega} - \frac{R_{ct}^2}{2} \right] + [Z'']^2 = \frac{R_{ct}^2}{4} \quad \longrightarrow \quad 3.37$$

which is the equation of a semicircle ( $Z''$  vs.  $Z'$  - constant concentration) with its center on the  $Z'$  axis at  $Z' = R_{\Omega} + 1/2 R_{ct}$  and radius  $1/2 R_{ct}$ . The interaction with the  $Z'$  axis are at  $Z' = R_{\Omega}$  for  $\omega = \infty$  and at  $Z' = R_{\Omega} + R_{ct}$  for  $\omega = 0$ . These are called Nyquist plots.

In a similar manner if we eliminate  $R_{ct}$  between  $Z'$  and  $Z''$

$$\left[ Z'' - \frac{1}{2\omega C_{dl}} \right]^2 + [Z' - R_{\Omega}]^2 = \frac{1}{4\omega^2 C_{dl}^2} \quad \longrightarrow \quad 3.38$$

which is the equation of a semicircular plot of  $Z''$  vs.  $Z'$  (constant frequency) with its centre on the  $Z''$  axis at  $\left[ R_{\Omega} + \frac{1}{2\omega C_{dl}} \right]$  and radius  $\frac{1}{2\omega C_{dl}}$ . Equation 3.37 represents a plot of  $Z''$  vs.  $Z'$  at various frequencies but at a fixed concentration of the electroactive species

or at a fixed concentration of inhibitor, which decides the concentration of electroactive species on electrode. The equation 3.38 represents the plot of  $Z''$  vs.  $Z'$  at different concentration but at a fixed frequency.

The two types of  $Z''$  vs.  $Z'$  plots are depicted below in Fig. vii.

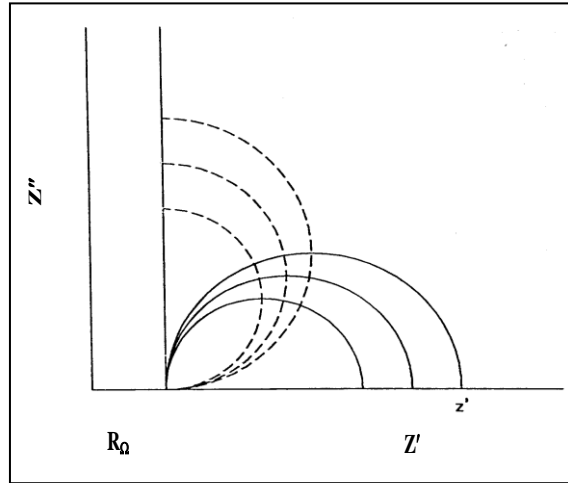


**Fig. vii: Electro impedance for various values of  $R_{ct}$  Dotted lines**

From the above theoretical aspects the following important conclusions and interpretations for current investigations could be made.

(i) If the corrosion process is purely diffusion controlled, the Nyquist plot will be a straight line with  $45^\circ$  slope. On the other hand, if the process is activation polarization controlled Nyquist plot will be semicircle with a radius of  $(R_{ct}/2)$  (Fig. viii).

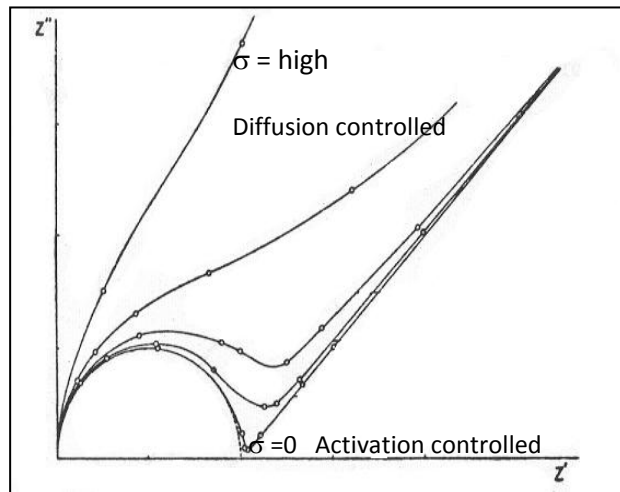


**Fig. viii: Effect of change in  $\sigma$  on the Nyquist**

For the present investigations all the Nyquist plots are semicircular in nature and hence all the inhibited systems in the current Chapter are activation controlled (Figs. 3.18 a-j).

(ii) As per equation 3.37 with the decrease in the concentration of the electroactive species on the electrode surface, the radius of the semicircle  $R_{ct}/2$  and hence  $R_{ct}$  will increase. This will happen if the metal surface is covered by adsorbed inhibitor molecules. Hence, an increase in  $R_{ct}$  with increase in inhibitor concentration will indicate an increase in inhibition efficiency (Table 3.10). This is what has been noticed in the current investigations.

(iii) From Fig. viii it is clear that with the increase in inhibitor concentration, the radius of the semicircle, equation 3.38 viz.,  $\frac{1}{2\omega C_{dl}}$  (which corresponds to the maximum for the Nyquist plot) also increases. This in turn would mean that the double layer capacitance  $C_{dl}$  decreases with increase in inhibitor (adsorbate) concentration. In the current investigations also  $C_{dl}$  decreases with increase in inhibitor concentration obviously due to increased adsorption and as required by theory.

These observations have been supported by the findings of **Selvaraj *et al.***,<sup>85-86</sup> in the study of effect of adsorption of ethanolamine (mono, di and tri) on the reduction of Pb(II) on dropping mercury electrode. It is also further supported by several investigations on corrosion<sup>87-90</sup>.

## (ii) Polarisation behaviour of inhibition

The polarization behaviour of inhibition could be better appreciated if the following theoretical aspects are considered.

According to **Frumkin**<sup>91,92</sup> the corrosion of a metal is decided by two important parameters viz., surface coverage  $\theta$  of electrode surface by inhibitor molecules / ions and the changes in  $\psi_1$  potential accompanying adsorption. The relation between  $\psi_1$  and  $\theta$  has been provided by the slow discharge theory<sup>93</sup> in the form of two rate expressions, one for cathodic evolution of hydrogen ( $i_c$ ) and another for anodic dissolution of metal ( $i_a$ ). They are,

$$i_c = k_1 [H_3O^+] (1-\theta) \exp \left\{ -\frac{F}{RT} \alpha \phi + (1-\alpha) \psi_1 \right\}$$

$$i_a = k_2 (1-\theta) \exp \left\{ \frac{F}{RT} 2\beta (\psi - \psi_1) \right\}$$

There are two cases of practical conditions, which alter the effect of inhibitors.

**Case 1: In the absence of oxygen or oxidizing inhibitors**

When inhibitors are added to a metallic system in corrosive environment without the presence of oxygen or oxidizing agents in solution, they may retard anodic and cathodic processes either separately or simultaneously. However, there is no guarantee that the adsorption of organic compounds would always lead to inhibition. This is because  $\psi_1$  and  $\theta$  may act in tandem or oppose each other, depending on the nature of the inhibitor. For the adsorption of cationic type of inhibitor, the effect of  $\psi_1$  and  $\theta$  are additive and the rate of corrosion decreases. In contrast, the adsorption of anionic type inhibitor may increase the velocity of corrosion if the corrosion processes are accelerated to a greater extent by the change of  $\psi_1$  potential than they are retarded by the increase of  $\theta$ . **Iofa *et al.***,<sup>94</sup> have observed this effect in the presence of various sulphanilic acids.

**Case 2: In the presence of oxygen or oxidizing inhibitors**

The presence of oxygen or other oxidizing agents in test solution may shift the stationary electrode potential leading to desorption of the inhibitor molecules. This is owing to either to the change of surface charge of the metal or to the removal of inhibitor molecules along with metal ions during dissolution of metal.

Inhibitors can be classified as anodic, cathodic or mixed type depending on the nature of alteration they make on polarization curves (Fig. ix).

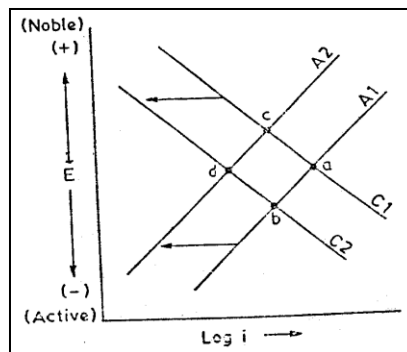


**Fig. ix. Diagrammatic representation of cathodic, anodic and mixed inhibitors**



Three types of inhibitors can be distinguished experimentally by their influence on the corrosion potential (Fig. ix). In the absence of any inhibitor, the cathodic and anodic polarization curves  $C_1$  and  $A_1$  intersect at point 'a' which corresponds to  $E_{\text{corr}}$ .

In the presence of cathodic inhibitor (which inhibit the cathodic process), the Tafel curve for cathode is shifted from  $C_1$  to  $C_2$  and the point of intersection to 'b', so that the corrosion potential  $E_{\text{corr}}$  moves in anodic (active) direction. Occasionally the Tafel slope  $b_c$  is altered as well.

An anodic inhibitor on the other hand alters the anodic polarization curve from  $A_1$  to  $A_2$  and the intersection to 'c', and the corrosion potential moves in the cathodic direction. With mixed type inhibitors, both cathodic and anodic polarization curves are shifted and the point of intersection becomes d. The change of corrosion potential is practically insignificant.

In the current studies, the presence of the isoxazolines shifts both anodic and cathodic branches to the lower values of current densities (Table 3.11) and thus causes a remarkable decrease in the corrosion rate. Oxygen is reduced in low cathodic overpotentials, but the main cathodic reaction in acidic solution is the discharge of hydrogen ions to produce hydrogen gas. It can be clearly seen from the (Figs. 3.19 b, c, e and i) that both anodic metal dissolution of iron and cathodic reactions were inhibited after the addition of isoxazolines to the aggressive solution. This result is indicative of the adsorption of inhibitor molecules on the active sites of mild steel surface<sup>95</sup>. The inhibition of both anodic and cathodic reactions is more pronounced with the increasing inhibitor concentration. However, the influence is more pronounced in the cathodic polarization plots compared to that of the anodic polarization plots. The cathodic current potential curves giving rise to parallel lines indicate that the addition of isoxazolines to the 1M  $\text{H}_2\text{SO}_4$  solution does not modify the reduction mechanism, and the reduction at mild steel surface takes place mainly through a charge transfer mechanism<sup>96-98</sup>. These results indicated that the presence of isoxazolines (ISO 2,3,5,9) inhibited iron oxidation and in a lower extent cathodic reduction reaction; Further inspection of the (Figs. 3.19 a, d, f, g and j) revealed that on increasing the concentration of isoxazolines (ISO 1,4,6,7,8,10) both anodic and cathodic current densities were shifted. Hence, it can be concluded that

all inhibitors can be classified as mixed corrosion inhibitors, as electrode potential displacement is lower than 85 mV in any direction.

### **3.5. Surface characterization**

#### **3.5.1 FTIR analysis of mild steel plate**

The mode of bonding of the isoxazolines to the mild steel surface was elucidated by comparing the FTIR spectra of the pure compounds with the IR spectra of the inhibited plates.

In the FTIR spectra of the inhibited plates (ISO 1,2,4,8) Table 3.12, (Figs. 3.20 - 3.23) the band around 3200 - 3300  $\text{cm}^{-1}$  attributed to N-H stretching vibrations have become weak (compared with the IR spectra of the isoxazolines) with reduced intensity which may be due to protonated NH group<sup>99</sup> and also confirming the adsorption of these compounds on mild steel surface *via.*, the protonated NH group. Presence of bands around 1627 - 1636  $\text{cm}^{-1}$ , 1310 - 1394  $\text{cm}^{-1}$  are characteristic of  $>\text{C}=\text{N}$  and  $>\text{C}-\text{O}-\text{N}$  stretching vibration frequencies, confirm the presence of isoxazolines on the metal surface.

In comparison to the FTIR spectrum of the inhibitors, it is evident that the  $>\text{NH}$ ,  $>\text{C}=\text{N}$ ,  $>\text{C}-\text{O}-\text{N}$  stretching frequency have shifted to a considerable extent and  $>\text{C}=\text{C}<$  stretching frequency of the aromatic ring have shifted drastically to the extent of 20 - 30  $\text{cm}^{-1}$  in comparison to the IR spectra of inhibitors confirming the active participation of the  $>\text{C}=\text{C}<$  in the adsorption process. Therefore, the shift in peak position of  $>\text{NH}$ ,  $>\text{C}=\text{N}$ , and  $>\text{C}-\text{O}-\text{N}$  in FTIR spectrum of mild steel immersed in 1M  $\text{H}_2\text{SO}_4$  containing inhibitors (ISO 1,2,4,8) as compared to the FTIR spectrum of pure compounds, clearly indicates the involvement of these groups of the inhibitors in the adsorption process on the metal surface.

#### **3.5.2 Scanning electron microscope-Energy dispersive X-Ray spectroscopy (SEM-EDS)**

Figs. 3.24 - 3.25 show the SEM micrographs of different slides of mild steel after immersion in the aqueous solution in the absence and presence of inhibitor (ISO 8). The exposure of mild steel sample to 1M  $\text{H}_2\text{SO}_4$  for 3 hours results in an aggressive attack of the corroding medium on the mild steel surface, strongly damaging the surface

(Fig. 3.24). SEM image of inhibited mild steel specimen (Fig. 3.25) reveals that a good protective adsorbed film of the inhibitor is formed on the specimen surface which suppresses the rate of corrosion.

The EDS spectra were used to determine the elements present on the surface of mild steel in the uninhibited and inhibited 1M H<sub>2</sub>SO<sub>4</sub>. The EDS analysis of uninhibited mild steel plate indicates the presence of only Fe and oxygen confirming that passive film on the mild steel surface contained only Fe<sub>2</sub>O<sub>3</sub> (Fig. 3.26). (Fig. 3.27) portrays the EDS spectra of mild steel in 1M H<sub>2</sub>SO<sub>4</sub> in the presence of isoxazoline (ISO 8). This EDS spectrum shows additional lines due to C, O and N. This spectrum confirms the presence of the isoxazolines molecules on mild steel surface<sup>100</sup>. A comparable elemental distribution is shown in Table 3.13.

### 3.5.3 X-ray diffraction patterns

XRD pattern represents the method of choice for the analysis of corrosion products, as it is the only analysis method that readily provides information about the phase-composition of solid materials. For instance, a mixture of Fe<sub>3</sub>O<sub>4</sub> (magnetite), FeO(OH) (goethite) and Fe<sub>5</sub>O<sub>7</sub>(OH)<sub>x</sub>.4H<sub>2</sub>O (ferrihydrite) can be identified and quantified as such, while other analysis methods will only reveal that the corrosion product is Fe-based. Furthermore, XRD can readily distinguish between different modifications of phases that have the same chemical formula. Goethite, lepidocrocite, feroxyhyte and akaganeite can be told apart, even though they all have the chemical formula FeO(OH)<sup>101</sup>. The XRD results are presented in Fig. 3.28-3.29. Peaks at  $2\theta = 29.8, 35.3$  and  $64.5^\circ$  are assigned to oxides of iron. The surface of the metal dipped in 1M H<sub>2</sub>SO<sub>4</sub> contains iron oxides, which are most probably Fe<sub>3</sub>O<sub>4</sub> (magnetite) and FeO(OH) (goethite) as shown for blank in Fig. 3.28. The XRD pattern for the metal dipped in 1M H<sub>2</sub>SO<sub>4</sub> containing optimum concentrations of the inhibitor (ISO 8) shows the intensity of the peaks due to oxides of iron such as Fe<sub>3</sub>O<sub>4</sub> and FeO(OH) are found to be very low as shown in Fig. 3.29 and the intensity of the peaks due to iron alone appeared at  $2\theta = 44.6, 65$  and  $82^\circ$  are very high. This confirms the protection of mild steel by ISO 8.

### 3.5.4 Atomic force microscopy

AFM is a powerful tool to investigate the surface morphology at nano to microscale levels. It has become a new method to investigate the nature of the protective layer formed on the mild steel surface<sup>102</sup>. AFM was used mainly for measuring the three dimensional topography. Figs. 3.30 and 3.31 shows the 2D and 3D AFM images of mild steel surface immersed in uninhibited and inhibited in the presence of an optimum concentration of the inhibitor (ISO 8). It is clear from the images that the surface of the specimen immersed in 1M H<sub>2</sub>SO<sub>4</sub> is offering more roughness when compared to the specimen immersed in the solution containing ISO 8. The average roughness of the mild steel immersed in 1M H<sub>2</sub>SO<sub>4</sub> was calculated as 145.71 nm whereas for the plate immersed in 1M H<sub>2</sub>SO<sub>4</sub> containing 10 mM (ISO 8), the roughness was calculated to be 26.37 nm. The decrease in the roughness value is ascribed to the formation of the protective layer of the inhibitor on the mild steel surface.

## 3.6 Quantum chemical studies

### 3.6.1 Quantum chemical study of non-protonated form of the studied inhibitors in aqueous phase

Quantum chemical calculations have proved to be a very powerful tool for studying corrosion inhibition mechanism<sup>103</sup>. Thus, a theoretical study was undertaken to observe the possible physical characteristics which would contribute to inhibition. Recently, the density functional theory (DFT) has been used to analyze the characteristics of the inhibitor/surface mechanism and to describe the structural nature of the inhibitor on the corrosion process<sup>104-107</sup>. Therefore, quantum chemical calculation using DFT was employed to explain the experimental results obtained in this study and to further give insight into the inhibition action of isoxazolines on the mild steel surface. The relation between inhibition efficiency of some selected isoxazolines and the calculated quantum chemical parameters like E<sub>HOMO</sub>, E<sub>LUMO</sub>, dipole moment, energy gap ( $\Delta E$ ), hardness, softness, electronegativity and the fraction of electrons transferred *etc.*, were investigated. These parameters provide information about the reactive behaviour of the molecules. These theoretical parameters were calculated in the non-protonated as well as in the protonated form of isoxazolines in the aqueous phase.

According to frontier molecular orbital theory (FMO), the chemical reactivity is a function of interaction between HOMO and LUMO levels of the reacting species<sup>108</sup>.  $E_{\text{HOMO}}$  is a quantum chemical parameter which is often associated with the electron donating ability of the molecule. High value of  $E_{\text{HOMO}}$  is likely to indicate a tendency of the molecule to donate electrons to appropriate acceptor molecule of low empty molecular orbital energy<sup>109</sup>. Therefore, the energy of the lowest unoccupied molecular orbital,  $E_{\text{LUMO}}$ , indicates the ability of the molecule to accept electrons<sup>110</sup>. So, the lower the value of  $E_{\text{LUMO}}$ , the more the probable the molecule would accept electrons. Thus the binding ability of the inhibitor to the metal surface increases with increasing of the HOMO and decreasing of the LUMO energy values. All the quantum chemical parameters for the non-protonated form of the inhibitors are given in Table 3.14.

According to Table 3.14, the total energy values which shows how stable the molecules are follow the trend ISO 1 < ISO 9 < ISO 7 < ISO 3 < ISO 2, which is the same order with the experimentally determined inhibition efficiency. The values of  $E_{\text{HOMO}}$  follow the order, ISO 7 > ISO 9 > ISO 3 > ISO 2 > ISO 1 which does not correlate with the experimentally determined inhibition efficiency. The values of  $E_{\text{LUMO}}$  follow the order, ISO 1 < ISO 9 < ISO 7 < ISO 2 < ISO 3 which deviates with the order of inhibition efficiency obtained experimentally.

The separation energy,  $\Delta E = (E_{\text{LUMO}} - E_{\text{HOMO}})$ , is an important parameter and it is a function of reactivity of the inhibitor molecule towards the adsorption on the metallic surface. As  $\Delta E$  decreases, the reactivity of the molecule increases leading to increase in the inhibition efficiency of the molecule<sup>111</sup>. The calculations from Table 3.14 show the decreasing trend for the property: ISO 1 < ISO 9 < ISO 7 < ISO 3 < ISO 2, which does not follow the same order of inhibition efficiency obtained for the inhibitors.

It is shown from the calculations that there is no obvious correlation between the values of the dipole moment with the trend of inhibition efficiency obtained experimentally. There is a lack of agreement in the literature on the correlation between the dipole moment and inhibition efficiency<sup>112, 113</sup>. Absolute hardness and softness are important properties to measure the molecular stability and reactivity. A hard molecule has a large energy gap and a soft molecule has a small energy gap. Soft molecules are more reactive than hard ones because they could easily offer electrons to an acceptor. For

the simplest transfer of electrons, adsorption could occur at the part of the molecule where,  $\sigma$  which is a local property, has the highest value<sup>114</sup>. In a corrosion system, the inhibitor acts as a Lewis base while the metal acts as a Lewis acid. Bulk metals are soft acids and thus soft base inhibitors are most effective for acidic corrosion of these metals. It is shown from the calculations that ISO 1 has the highest hardness and the lowest softness which deviates from the expected trend from the experimental inhibition efficiency obtained. Normally, the inhibitor with the least value of global hardness (hence the highest value of global softness) is expected to have the highest inhibition efficiency<sup>115</sup>.

The number of electrons transferred ( $\Delta N$ ) was also calculated and tabulated in Table 3.14. Values of  $\Delta N$  show that the inhibition efficiency resulting from electron donation agrees with Lukovit's study<sup>116</sup>. If  $\Delta N < 3.6$ , the inhibition efficiency increases by increasing electron-donating ability of these inhibitors to donate electrons to the metal surface and it increases in the following order ISO 9 > ISO 7 > ISO 3 > ISO 1 > ISO 2. The results indicate that  $\Delta N$  values across the structures do not correlate well with the trend in the experimentally determined inhibition efficiency. The optimized geometries, HOMO and LUMO of the isoxazoline derivatives in non-protonated form in aqueous phase are shown in Table 3.16.

### **3.6.2 Quantum chemical study of protonated form of the studied inhibitors in aqueous phase**

Organic inhibitors under investigation have a great tendency to be protonated in acidic medium due to the presence of N atoms. This is confirmed from the calculations which show the greater stability of protonated inhibitors (Table 3.17). It is shown from the optimized structures of the investigated inhibitors that there are one or more active centers on the inhibitor for protonation.

Most of the quantum chemical parameters/descriptors calculated in the protonated form such as total energy,  $E_{\text{HOMO}}$ ,  $E_{\text{LUMO}}$ , energy gap ( $\Delta E$ ), hardness, softness and fraction of electrons transferred were in accordance with the order of inhibition efficiency obtained experimentally ISO 2 > ISO 3 > ISO 7 > ISO 9 > ISO 1. These results demonstrate that in acid medium, the protonated form of the inhibitors should make a

higher contribution to the corrosion inhibiting effect of the isoxazolines on the mild steel surface.

Comparison of quantum chemical calculations for protonated and non-protonated inhibitors indicates that there is a clear correlation between most of the quantum chemical parameters/descriptor in the protonated form and non-protonated form of the studied isoxazoline derivatives in aqueous phase (Table 3.14 and 3.17).

Table 3.16 and Table 3.19 show the HOMO and LUMO orbital contributions for the non-protonated and protonated species of the studied molecules respectively. For the studied inhibitors, the HOMO densities were concentrated on the isoxazoline ring in the neutral form while the protonated form has the HOMO mainly on the substituents. For the LUMO distributions the reverse is the case.

Thus unoccupied orbitals of Fe atom can accept electrons from inhibitor molecule both in the non-protonated and protonated species to form a coordinate bond. Also the inhibitor molecule can accept electrons from Fe atom with its anti bonding orbitals to form back-donating bond. These donation and back donation processes strengthen the adsorption of these inhibitors onto the mild steel surface.

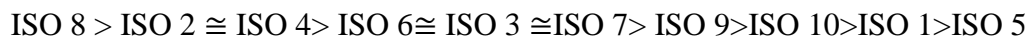
### **3.6.3 Mulliken charge density distribution**

The Mulliken charge distributions for non-protonated and protonated forms are presented in Table 3.15 and 3.18. It has been reported that the more negative the atomic charges of the adsorbed center, more easily the atom can donate its electrons to the unoccupied orbital of the surface of the metal atoms. In non-protonated forms, nitrogen and oxygen atoms have higher charge densities, *i.e.*, N1, N16 (ISO 1) and N1, N13 (ISO 2, 3, 7, 9) as shown in Table 3.15. The regions of the highest electron density are generally the sites to which electrophiles attack. Therefore N atoms are the active centers, which have the strongest ability of bonding to the metal surface. In protonated form oxygen and some carbon atoms have negative charge and they are capable of bonding to the metal surface. On the other hand, nitrogen and some carbon atoms carry positive charges, which are sites to which nucleophiles can attack. Therefore, isoxazolines can accept electrons from Fe through these atoms. It has been reported that excellent corrosion inhibitors can not only offer electrons to unoccupied orbital of the metal, but also accept free electrons from the metal. These strengthen the adsorption of the

isoxazolines on the mild steel surface leading to a stable protective layer and thus retarding further corrosion of the metal in sulphuric acid solution.

### 3.7 Evaluation of isoxazolines: Chemical structure and corrosion inhibition of Fe

The inhibition efficiency of the isoxazolines follows the order:



The inhibition efficiency of the investigated compounds depend on many factors, which include the number of adsorption active centres in the molecule and their charge density, molecular size, mode of adsorption, heat of hydrogenation and formation of metallic complexes.

The inhibition efficiency of the investigated isoxazolines at 10 mM is in the range 83 – 98 % except ISO 5 with 67 %. The higher inhibition efficiency of these compounds in general is due to the presence of aromatic rings, >C=N- groups, -NH and electron donating substituents in the aromatic ring such as OH, OCH<sub>3</sub>, NMe<sub>2</sub> which enhances the electron density of the aromatic ring leading to greater adsorption.

ISO 8 has the highest percentage inhibition efficiency (98 %). This may be due to the presence of a naphthyl ring. -OH group in ortho position is expected to form intramolecular hydrogen bond with lone pair of electrons on oxygen of isoxazoline ring leading to the less availability of lone pair of electron on oxygen for electrostatic interaction with metal due to ortho effect. In contradiction, the high inhibition efficiency of ISO 8 indicates that -OH group is not in the same plane as naphthyl ring and does not form hydrogen bond with the isoxazoline ring oxygen. Therefore the lone pair of electrons on the ring oxygen atom of isoxazoline also acts as anchoring site and enhances the percentage inhibition efficiency. ISO 2 and ISO 4 have almost equal IE of about 96 % which may be attributed to the presence of three methoxy groups (p-OCH<sub>3</sub>,  $\sigma = -0.27$ ) and two methoxy groups respectively. They are all electron donating groups with negative Hammett constant which enhance the electron density on the molecule. As the number of electron donating groups on the benzene ring increases percentage inhibition efficiency also increases. The superior performance of methoxy derivatives can be explained on the basis of Pearson HSAB principle<sup>117</sup> according to which the methoxy derivatives is considered as a hard base which forms strong bond with ferrous and ferric iron which is a soft base. This leads to higher adsorption and greater inhibition.



ISO 6, ISO 3 and ISO 7 have almost same percentage inhibition efficiency of 94%. ISO 6 is expected to show very high inhibition efficiency due to the presence of  $-NMe_2$  group (Hammett constant  $\sigma = -0.83$ ) but it is slightly less than expected. This may be due to the out of plane orientation of  $-NMe_2$  with respect to benzene ring thus preventing the exactly flat orientation of the molecule onto the mild steel surface. ISO 3 has  $m-OCH_3$  group ( $\sigma = +0.115$ ) and  $p-OH$  group ( $\sigma = -0.37$ ) in which the effect of  $m-OCH_3$  has probably overcome the effect of  $p-OH$  group leading to a slight decrease in inhibition efficiency. In general there is a greater tendency for the dissolution of hydroxy compounds in aqueous acid medium leading to the dissolution of inhibitor film from the metal surface. This is supported by the finding of **Quraishi *et al.***,<sup>118</sup>.

ISO 10 has a  $p-Cl$  group ( $\sigma = +0.227$ ), it has a +I effect, hence tends to decrease the electron density on benzene ring to some extent leading to a decrease in inhibition efficiency. Finally compound ISO 5 has the least IE of 67 % which may be attributed to the strong electron withdrawing nature of the  $NO_2$  group which reduces the electron density on the molecule and thereby result in a decrease in protection efficiency.

### 3.8 CONCLUSIONS

- All the isoxazolines studied are found to perform well as corrosion inhibitors in 1M  $H_2SO_4$  and the inhibition efficiency values of the examined isoxazolines follow the order:  
ISO 8 > ISO 2  $\cong$  ISO 4 > ISO 6  $\cong$  ISO 3  $\cong$  ISO 7 > ISO 9 > ISO 10 > ISO 1 > ISO 5
- They inhibit corrosion by getting adsorbed on the mild steel surface. The inhibition efficiency increases with increase in inhibitor concentration.
- The adsorption of the compounds on metal surface is found to obey Langmuir adsorption isotherm.
- The inhibition efficiency obtained from the atomic absorption spectrophotometric studies was found to be in good agreement with that obtained from the conventional weight loss method.
- The activation energy is higher for the inhibited acids than for uninhibited acids showing the temperature dependence of inhibition efficiency.

- The negative values of standard free energy of adsorption  $\Delta G_{\text{ads}}^{\circ}$  confirm the spontaneity of the adsorption process.
- Polarization studies showed that all the isoxazolines function as mixed inhibitors but predominantly act as cathodic inhibitors.
- SEM reveals the formation of a smooth, dense protective layer in presence of an effective inhibitor.
- FTIR, XRD and AFM spectra results supported the adsorption of the isoxazoline molecules on the mild steel surface.
- Results obtained from quantum mechanical studies for some of the protonated isoxazoline derivatives were found to be in good agreement with the experimental results.

### 3.9 REFERENCES

1. D. Jayaperumal, Mater. Chem. Phys., **119** (2010) 478.
2. S.S. Abdel-Rehim, K.F. Khaled, N.A. Al-Mobarak, Arab. J. Chem., **4** (2011) 333.
3. S.A. Umoren, I.B. Obot, E.E. Ebenso, N.O. Obi-Egbedi, Desalination., **250** (2009) 225.
4. M. Bouklah, B. Hammouti, A. Aouniti, T. Benhadda, Prog. Org. Coat., **49** (2004) 225.
5. K. Tebbji, A. Aouniti, M. Benkaddour, H. Oudda, I. Bouabdallah, B. Hammouti, Prog. Org. Coat., **54** (2005) 170.
6. I.A. Zaafarany, Int. J. Electrochem. Sci., **8** (2013) 9531.
7. C.E. Winter, E.A. Risley, G.W. Nuss, Proc. Soc. Exp. Bio. Med., **111** (1962) 544.
8. I.N. Levin, Quantum chemistry (New Jersey: Prentice hall) (1991).
9. N.S. Patel, S. Jauhari, G. N. Mehta, Acta. chim. slov., **57** (2010) 297.
10. P.C. Sharma, S.V. Sharma, S. Jain, D. Singh, B. Suresh, Acta. Pol. Pharm., **66** (2009) 101.
11. A.S. Fouda, M.A. Elmorsi, A. Elmekawy, Int.J. Electrochem. Sci., **7** (2013) 337.
12. N.O. Eddy, E.E. Ebenso, U.J. Ibok, E.E. Akpan, Int. J. Electrochem. Sci., **6** (2011) 4296.
13. A.K. Chandra, M.T. Nguyen, Int. J. Mol. Sci., **3** (2002) 310.
14. P.Geerlings, F. De Proft, W. Langenaeker, Chem. Rev., **103** (2003) 1793.
15. R.G. Parr, R.G. Pearson, J. Am. Chem. Soc., **105** (1983) 7512.
16. L. Pauling, The nature of the chemical bond (Cornell University Press, Ithaca, New York, (1960)
17. R.G. Parr, L. Szentpaly, S. Liu, J. Am. Chem. Soc., **121** (1999) 1922.
18. I. Lukovits, E. Kalman, F. Zucchi, Corros., **57** (2001) 3.
19. R.G. Pearson, Inorg. Chem., **27** (1988)734.
20. V.S. Sastri and J.R. Perumareddi, Corros. Sci., **53** (1997) 617.
21. M.J.S. Dewar, W. Thie, J. Am. Chem. Soc., **99** (1977) 4899.
22. H. Asharri-Sorkhabi, N. Ghalebsaz-Jeddi, F. Hashemzadeh, H. Jahani, Electrochimica. Acta., **51** (2006) 3848.
23. T. Tsuru, S. Haruyama, B. Gijutsu, J. Jpn. Soc. Corros. Eng., **27** (1978) 573-581.

24. Z.A. Iofa, V.V. Batrakov, C. Ngor, Ba. Zashchita Metallov., (1965) 56.
25. J.O.M. Bockris, D.A. Swinkels, J. Electrochem. Soc., **111** (1964) 736.
26. J.O.M. Bockris, M. Green, D.A. Swinkels, J. Electrochem. Soc., **111** (1964) 743.
27. B.B. Damaskin, O.A. Petrii, V.V. Batrakov, Adsorption of Organic compounds on electrodes, Plenum Press, New York, London, (1971) 257.
29. A.N. Frumkin, Vestn. Mosk. Gos. Univ., **9** (1952) 37.
30. Z.A. Iofa, Vestn. Mosk. Gos. Univ., **2** (1956) 139.
31. A.C. Mackrides, N. Hackerman, Ind. Eng. Chem., **47** (1955) 1773.
32. E.L. Look, N. Hackerman, J. Phys. Colloid Chem., **55** (1951) 549.
33. N. Hackerman, A.C. Makrides, Ind. Eng. Chem., **46** (1964) 523.
34. C.C. Nathan, Corros., **12** (1956) 1610.
35. E.B. Greenhill, Trans. Faraday Soc., **45** (1949) 625.
36. F.P. Bowden, A.C. Moore, Trans. Faraday Soc., **47** (1951) 900.
37. L. Cavallaro, G.P. Bolognesi, Atti. Acad. Sci. Ferrara., **24** (1946-47) 235.
38. G.L. Foster, B.D. Oaker, C.H. Kucera, Ind. Eng. Chem., **51** (1959) 825.
39. I.N. Putilova, A.M. Lolva, I.I. Suponitskaya, G.M. Maslova, Zashchita. Metallov., **4** (1968) 392.
40. V.V. Losev, B.N. Kabanov, Izv. Akad. Nauk SSR, Otd. Khim. Nauk, (1957) 414.
41. W. Machu, Korros. Metallschutz., **10** (1934) 277.
42. S.D. Levina, Zh. Prikl. Khim., **29** (1958) 1353.
43. L. Horner, A. Mentrup, Liebigs Ann. Chem., **65** (1961) 646.
44. F. Bottger, H. Fuchs, L. Horner, Chem. Ber., **96** (1963) 3141.
45. H.M. Bhajiwala, R.T. Vashi, Bull. Electrochem., **17** (2001) 441.
46. D.P. Schweinsberg, G.A. George, A.K. Nanayakkara, D. Steinert, Corros. Sci., **28** (1998) 3.
47. A.S. Fouda, M.N. Moussa, Fl Taha, Al Elneanaa, Corros. Sci., **26** (1986) 719.
48. J.K. Sahu, K.K. Sahu, A.K. Ray, Proceedings of the institution of mechanical engineers Part L-Journal of materials-Design and applications, **226** (2012) 34.
49. A. Jamal Abdul Nasser, M. Anwar Sathiq, Int. J. Eng. Sci. Tech., **2** (2010) 6417.
50. A. Popova, E. Sokolova, S. Raicheva, M. Christov, Corros. Sci., **45** (2003) 33.
51. N.O. Obi-Egbedi, I. B. Obot, Corros. Sci., **53** (2011) 850.

52. M.A. Quraishi, S. Khan, *Ind. J. Chem. Tech.*, **12** (2005) 576.
53. C.B. Breslin, W.M. Carrol, *Corros. Sci.*, **34** (1993) 327.
54. M.G.A. Khedr, M. S. Lashien, *Corros. Sci.*, **33** (1992) 137.
55. N.A. Negm, M.F. Zaki, *Colloid Surf. A: Physiochem. Eng. Aspec.*, **322** (2008) 97.
56. N.A. Negm, M. A. I. Salem, M. F. Zaki, *J. Dis. Sci. Tech.*, **30** (2009) 1167.
57. L. Labrabi, Y. Harek, O. Benali, S. Ghalem, *Prog. Org. Coatings.*, **54** (2005) 256.
58. E.E. Oguzie, *Mater. Chem. Phys.*, **99** (2006) 441.
59. T.P. Hoar, R.D. Holliday, *J. Appl. Chem.*, **3** (1953) 502.
60. L. Riggs Jr, M. Hurd, *Corrosion.*, **23** (1967) 252.
61. G.M. Schmid, H.J. Huang, *Corros.Sci.*, **20** (1980) 1041.
62. M.A. Hegazy, M. F. Zaky, *Corros.Sci.*, **52** (2010) 1333.
63. Y. Abboud, A. Abourriche, T. Saffaj, M. Berrada, M. Charrouf, A. Bennamara, N.Al Himidi, H. Hannache, *Mater. Chem. Phys.*, **105** (2007) 1.
64. G. Quartarone, G. Moretti, A. Tassan, A. Zingales, *Mater. Corros.*, **45** (1994) 641.
65. M.R. Arshadi, M. Lashgari, Gh.A. Parsafar, *Mater. Chem. Phys.*, **86** (2004) 311.
66. M. Christov, A. Popova, *Corros. Sci.*, **46** (2004) 1613.
67. F. Bentiss, M. Traisnel, L. Gengembre, M. Lagrenee, *Appl. Surf. Sci.*, **152** (1999) 237.
68. B.B. Damaskin, O.A. Petrii, B. Batrakov, Plenum Press, New York, 1971.
69. I. Langmuir, *J. Am. Chem. Soc.*, **39** (1917) 1848.
70. R. Alberty, R. Silbey, *Physical Chemistry*, second ed., Wiley, New York (1997) 845.
71. O. Volk, H. Fischer, *Electrochem. Acta.*, **4** (1961) 112.
72. R. Annand, R.M. Hurd, N. Hackerman, *J. Electrochem. Soc.*, **112** (1965) 138.
73. E.E. Ebenso, *Mater. Chem. Phys.*, **79** (2003) 58.
74. S.S. Abd El. Rehim, M.A.M. Ibrahim, K.F. Khaled, *J. Appl. Electrochem.*, **29** (1999) 593.
75. O. Olivares, N.V. Likhanova, B. Gomez, J. Navarrete, M.E. Llanos-Serrano, E. Arce, J.M. Hallen, *Appl. Surf. Sci.*, **252** (2006) 2894.
76. B.B. Damaskin, O.A. Petrii, V.V. Batrakov, *Adsorption of organic compounds on electrodes*, Plenum press, New york, London, (1971) 245.

77. L.D. Mall, V.C. Srivastava, N.K. Agrawal, I.M. Mishra, *Colloids Surf. A: Physicochem. Eng. Aspects.*, **264** (2005) 17.
78. N.O. Obi-Egbedi, I.B. Obot, *Corros. Sci.*, **53** (2011) 263.
79. X.H. Li, S.D. Deng, H. Fu, G.N. Mu, *Corros.Sci.*, **50** (2008) 2635.
80. T.P. Zhao, G.N. Mu, *Corros. Sci.*, **4** (1999) 1937.
81. W. Durnie, R. De Marco, B. Kinsella, A. Jefferson, *J. Electrochem. Soc.*, **146** (1999) 1751.
82. A. Zarrouk, B. Hammouti, H. Zarrok, S.S. Al-Deyab, M. Messali, *Int. J. Electrochem. Sci.*, **6** (2011) 6261.
83. J.E.B. Randles, *Disc. Faraday Soc.*, **1** (1947) 11.
84. P. Delahay, *J. Phy. Chem.*, **70** (1996) 2373.
85. J.H. Sluyters, *RECUEIL*, **79** (1960) 1092.
86. A. Selvaraj, R.S. Subrahmanya, *J. Electrochem. Soc.*, **32(36)** (1988) 193.
87. A. Selvaraj, R.S. Subrahmanya, *J. Electrochem. Soc.*, **32(36)** (1987) 225.
88. S. Rajendran, V. Gangasri, J. Arockiaselvi, A. John Amalraj, *Bull. Electrochem.*, **21** (2005) 367.
89. M.A. Quraishi, F.A. Ansari, *Bull. Electrochem.*, **22(1)** (2006) 35.
90. V. Violet Dhayabaran, A. Rajendran, P. Suganya, *Bull. Electrochem.*, **22** (2006) 43.
91. O. Olivares-Xomet, N.V. Likhanova, M.A. Dominguez-Aguilar, J.M. Hallen, L.S. Zamudio, E. Arce, *Appl. Surf. Sci.*, **252** (2006) 2139.
92. A.N. Frumkin, *Electrochim. Acta*, **9** (1964) 465.
93. A.N. Frumkin, Fundamental problems of modern theoretical electrochemistry, Proceedings of the 14<sup>th</sup> CITCE meeting [in Russian], Izd "Mir" Moscow (1965) 302.
94. A.N. Frumkin, V.S. Bagotskii, Z.A. Iofa, B.N.Kabanov, Kinetics of electrode processes [in Russian] Izd. Mosk. Gos. Univ., Moscow (1952).
95. Z.A. Iofa, Proceedings of the second european symposium on corrosion inhibitors, Ferrara, Ann. Univ. Ferrara, **151** (1965).
96. H. Ashassi-Sorkhabi, B. Shaabani, D. Seifzadeh, *Appl. Surf. Sci.*, **239** (2005) 154.
97. R. Fletcher, Practical methods of optimization, Vol I. Wiley, New York (1980)
98. A. Chetouani, B. Hammouti, T. Benhadda, M. Daoudi, *Appl. Surf. Sci.*, **249** (2005) 375.

99. A. Chetouani, A. Aouniti, B. Hammouti, N. Benchat, T. Benhadda, S. Kertit, *Corros. Sci.*, **45** (2003) 1675.
100. Y. Abboud, B. Hammouti, A. Abourriche, B. Ihssane, A. Bennamara, M. Charrouf S.S. Al-Deyab, *Int. J. Electrochem. Sci.*, **7** (2012) 2543.
101. S. Fouda, A.F. Hassan, M.A. Elmorsi, T.A. Fayed, A. Abdelhakim, *Int. J. Electrochem. Sci.*, **9** (2014) 1298.
102. T. Kamimura, S. Nasu, T. Tazaki, K. Kuzushita, S. Morimoto, *Mater. Trans.* **43** (2002) 694.
103. M.A. Quaraishi, A. Singh, V. Singh, D. Yadav, A.K. Singh, *Mater.Chem. Phys.*, **122** (2010) 114.
104. N.O. Obi-Egbedi, I.B. Obot, *Arab. J. Chem.*, (2010) doi:10.1016/Jarabic.
105. M. Lashkari, M.R. Arshadi, *J. Chem. Phys.*, **299** (2004) 131.
106. T.L. Sein, Y. Wei, S.A. Jansen, *Comput. Theor. Polym. Sci.*, **11** (2001) 83.
107. E.E. Ebenso, T. Arslan, F. Kandemirli, N. Caner, I. Love, *Int. J. Quant. Chem.*, **110** (2010) 1003.
108. A.Y. Musa, A.H. Kadhum, A.B. Mohamad, A.B. Rohoma, H. Mesmari, *J. Mol. Struct.*, **969** (2010) 233.
109. G. Gece, S. Bilgic, *Corros. Sci.*, **51** (2009) 1876.
110. I. Ahamad, R. Prasad, M.A. Quarishi, *Corros.Sci.*, **52** (2010) 1472.
111. M.K. Awad, M.R. Mustafa, M.M. Abo Elnga, *J. Mol. Struct. (THEOCHEM)* **959** (2010) 66.
112. L.M. Rodrigez-Valdez, A. Martinez-Villfane, D. Glossman-Mitnik, *J. Mol. Struct., (THEOCHEM)* **713** (2005) 65.
113. A. Stoyanova, G. Petkova, S.D. Peyerimhoff, *Chem. Phys.*, **279** (2002) 1.
114. R. Hasanov, M. Sadikglu, S. Bilgic, *Appl.Surf.Sci.*, **253** (2007) 3913.
115. E.E. Ebenso, D.A. ISabirye, N.O. Eddy, *Int.J. Mol. Sci.*, **11** (2010) 2473.
116. I. Lukovits, E. Kalman, F. Zucchi, *Corrosion (NACE)* **57** (2001) 3.
117. M.A. Quaraishi, M.A. Wajid Khan, M. Ajmal, S. Muralidharan, S.Venkatakrishna Iyer, *J. Appl. Electrochem.*, **26** (1996) 1253.
118. S. Muralidharan, M.A. Quraishi, S.V.K. Iyer, *Corros. Sci.*, **37** (1995) 1739.